Amorphous–nanocrystalline alloys fabrication, properties, and applications

Li, F.C.; Liu, T.; Zhang, J.Y.; Shuang, S.; Wang, Q.; Wang, A.D.; Wang, J.G.; Yang, Y.

Published in:
Materials Today Advances

Published: 01/12/2019

Document Version:
Final Published version, also known as Publisher's PDF, Publisher's Final version or Version of Record

Published version (DOI):
10.1016/j.mtadv.2019.100027

Publication details:
Li, F. C., Liu, T., Zhang, J. Y., Shuang, S., Wang, Q., Wang, A. D., Wang, J. G., & Yang, Y. (2019). Amorphous–nanocrystalline alloys: fabrication, properties, and applications. *Materials Today Advances*, *4*, [100027]. https://doi.org/10.1016/j.mtadv.2019.100027

Materials Today Advances 4 (2019) 100027

Contents lists available at ScienceDirect

Materials Today Advances

journal homepage: www.journals.elsevier.com/materials-today-advances/

Amorphous–nanocrystalline alloys: fabrication, properties, and applications

F.C. Li [a], T. Liu [a, b], J.Y. Zhang [a], S. Shuang [a], Q. Wang [c], A.D. Wang [a], J.G. Wang [a, d], Y. Yang [a, e, *]

[a] Department of Mechanical Engineering, College of Engineering, City University of Hong Kong, Kowloon Tong, Kowloon, Hong Kong Special Administrative Region, China
[b] The State Key Laboratory of Refractories and Metallurgy, Wuhan University of Science and Technology, Wuhan, 430081, China
[c] Laboratory for Structures, Institute of Materials Science, Shanghai University, Shanghai, 200072, China
[d] College of Mechanical Engineering, Dongguan University of Technology, Dongguan, 523808, China
[e] Department of Materials Science and Engineering, College of Engineering, City University of Hong Kong, Kowloon Tong, Kowloon, Hong Kong Special Administrative Region, China

ARTICLE INFO

Article history:
Received 25 August 2019
Received in revised form
14 October 2019
Accepted 21 October 2019
Available online 26 November 2019

Keywords:
Amorphous alloys
Nanocrystalline alloys
Metallic glasses
Composites

ABSTRACT

Owing to their unique mechanical and functional properties, both amorphous and nanocrystalline alloys have attracted extensive research interest over the past decades. However, in spite of the tremendous efforts dedicated to both kinds of alloys, their engineering applications are still hindered today because some fundamental issues, such as low thermal stability and poor ductility, are yet to be solved. To overcome these issues, one recent strategy proposed is to combine both amorphous and nanocrystalline structures in a single alloy through the use of either an amorphous or a nanocrystalline alloy as a "template". On the one hand, the derived amorphous–nanocrystalline alloys may inherit the unique properties from either the amorphous or the nanocrystalline "template", such as outstanding magnetic properties, extraordinary wear/corrosion resistance, and superior hardness and strength. On the other hand, these amorphous–nanocrystalline alloys also exhibit enhanced thermal stability and ductility, which are difficult to achieve for either the amorphous or the nanocrystalline alloy template. In this review article, we would like to first discuss a number of experimental methods developed to fabricate amorphous–nanocrystalline alloys, including partial crystallization in amorphous precursors, grain boundary amorphization, and physical vapor deposition. After that, we will give an overview of the mechanical and functional properties of the amorphous–nanocrystalline alloys. Finally, we will have a discussion on the existing applications of the amorphous–nanocrystalline alloys in various areas such as renewable and green energy, catalysis, and surface protection.

1. Introduction

An amorphous–nanocrystalline alloy is generally a dual-phase material made up of a metallic amorphous phase and nano-sized crystals. On the one hand, amorphous metals, which lack long-range translational symmetry and crystalline defects, possess large elastic strain limit, superb strength, excellent thermo-plastic formability, and good corrosion/wear resistance [1–4]. On the other hand, nanocrystalline metals, with their grain size falling into the nanometer range (<100 nm) [1], also exhibit a unique combination of enhanced mechanical, chemical, and physical properties such as high strength, superior catalytic properties, and abnormal thermal properties [2–4]. Since the advent of amorphous alloys over six decades ago [5], their development has been attracting tremendous research interest. In the first decade or so, the research on amorphous alloys was mainly focused on a few binary and ternary systems with a rather limited size [6–8]. With the development of new techniques [9,10] and theories [11–14], a large number of multicomponent systems, such as Zr- [15,16], Mg- [17], La- [18], Ti- [19], Fe- [20], Co- [21] and Ni-based [22] amorphous alloys, were developed in the 1990s, which had a good glass-forming ability (GFA) and could be cast into fully glassy rods with diameters ranging from several millimeters to centimeters

* Corresponding author.
E-mail address: yonyang@cityu.edu.hk (Y. Yang).

https://doi.org/10.1016/j.mtadv.2019.100027

[14,23–25]. Compared to conventional alloys, amorphous alloys were once considered alternative structural alloys owing to their high strength and good fracture toughness [26]. However, their structural applications are much hindered even today because of their poor ductility [27]. Apart from their structural applications, amorphous alloys have various functional applications, such as electrochemical hydrogen generation [28], azo dye degradation for decorations, and other purposes [29].

Nanocrystalline alloys, as defined early by Gleiter [1] in 1989, are simply a metal with nano-sized grains. Since the first report of bulk nanocrystalline alloy by Birringer in 1984 [30], many methods have been developed and explored to make nanocrystalline alloys, including the ball milling method [31], full crystallization of amorphous alloys [32], ultrasonic shot peening method [33], surface mechanical attrition method [34] and electrodeposition and sputtering methods [35,36]. Compared to coarse-grained metals, nanocrystalline metals possess high strength and hardness but poor thermal stability at a high temperature [37,38] and brittleness at a low temperature [4,39].

To overcome the shortcomings and enhance the properties of nanocrystalline or amorphous alloys, one strategy proposed is to combine these two together to form amorphous–nanocrystalline alloys. Early in the 1970s, annealing-induced nanocrystallization was already observed in a number of amorphous alloys, such as Pd–Si, Fe–P–C, and Fe–Si–B [40–43]. With the formation of these nanocrystals, the physical and chemical properties of the original amorphous precursors could be improved [44–46], such as the soft magnetic Fe-based amorphous–nanocrystalline alloys [47]. Aside from thermal annealing of amorphous alloys, amorphous–nanocrystalline alloys could also be obtained directly through electrodeposition and magnetic sputtering [48]. This provides a convenient route for the in-situ formation of amorphous–nanocrystalline alloys, which was already demonstrated in Al–Mo [49], Cu–Zr [50] and Mg–Cu–Y [51] obtained via magnetic sputtering or Al–Mn [52] and Ni–W [53] obtained via electrodeposition. Notably, these amorphous–nanocrystalline thin films could have many potential applications, such as for surface protection and in nano-devices [54].

Alternatively, amorphous–nanocrystalline alloys can be obtained by grain boundary (GB) amorphization in nanocrystalline alloys. In 2015, Khalajhedayati and Rupert [55] reported the formation of amorphous intergranular films in a Cu–Zr nanocrystalline alloy via thermal annealing, which was due to solute segregation in grain boundaries. As a result, the thermal stability of nanocrystalline alloys could be improved as well as their ductility and fracture toughness [56,57]. To facilitate our understanding, Fig. 1 illustrates the historic development of the techniques that were used for obtaining amorphous–nanocrystalline alloys. As seen in this figure, soon after the discovery of the first amorphous alloy by Klement et al. [5] in 1960, the first amorphous–nanocrystalline alloy was already obtained by Chen et al. [58] in 1969 through thermal annealing. After that, Ruan and Schuh [52] obtained an amorphous–nanocrystalline thin film through electrodeposition in 2009. Relatively speaking, it is a recent development to obtain amorphous–nanocrystalline alloys through GB amorphization. The first report might be due to the work of Khalajhedayati et al. in 2015 [55]. In this review article, our goal is to provide a comprehensive and up-to-date understanding of the development and properties of amorphous–nanocrystalline alloys obtained via various means, such as thermal annealing, GB segregation and amorphization, physical vapor deposition (PVD), and electrodeposition. In addition, we would like to also highlight a few important and interesting applications of amorphous–nanocrystalline alloys in recent years.

2. Fabrication methods

2.1. Controlled nanocrystallization in amorphous alloys

To form nanocrystalline amorphous alloys out of monolithic amorphous alloys, several approaches have been developed over the past decades, which include furnace or flash annealing (Joule heating [59] and micro-wave heating [60]), severe plastic deformation (high-pressure torsion [61], cold rolling [62], shot peening [63,64] and ball milling [65]), irradiation by electrons [66,67], ions [68] or pulsed laser [69] and ultrasound vibration [70]. Among these methods, annealing-induced crystallization is most attractive because of its easy control. In principle, crystallization is associated with the nucleation and growth of crystallites. Therefore, there are two basic mechanisms to form nanocrystalline amorphous alloys. As shown in Fig. 2a, the first type is associated with a good glass former, which affords relatively slow cooling. However, if it is cooled at a relatively fast cooling rate, say, 10^3 K/s, crystallite nucleation can be bypassed, leaving a monolithic amorphous structure without quenched-in nuclei. In such a case, one can easily distinguish glass transition from crystallization on the typical DSC trace of the corresponding amorphous alloy and subsequent annealing can cause nanocrystallization [14,71,72]. In contrast, the second type is associated with a marginal glass former, in which the nucleation of crystallites can be hardly bypassed but their growth is really slow (Fig. 2b). Therefore, further growth of the quenched-in crystalline nuclei can be triggered in this type of amorphous alloy upon reheating. On the typical DSC trace of these amorphous alloys, the signal of glass transition is usually missing [73,74].

Many Zr-based amorphous alloys, such as $Zr_{41.2}Ti_{13.8}Cu_{12.5}Ni_{10}Be_{22.5}$ (Vit1), are good or bulk glass formers, which can be used to make the first type of nanocrystalline amorphous alloy. In these glass-forming alloys, crystallization becomes difficult because of the presence of some local geometric short-range orders (SROs), such as icosahedral clusters, which is however not compatible with a space-filling topology and hence cannot directly lead to overall crystallization in most cases. According to Xing et al. [75] and Cang et al. [76,77], these icosahedral clusters can facilitate nanocrystallization by serving as the potential sites for heterogeneous nucleation of primary crystals. However, based on a thorough TEM study, Wang et al. [78] proposed that nanocrystalline can be also facilitated by the icosahedral clusters because of a “pinning” effect. As a crystallite grows outward from its nucleus, its growth is retarded once its boundary is pinned by the surrounding icosahedral clusters, as illustrated in Fig. 3. Once the density of the icosahedral clusters reaches 10^{24}–10^{25} m^{-3} [79], a high density of nanocrystals can form in these bulk glass formers. According to Ref. [80], the volume fraction of the nanocrystals obtained by annealing a Zr-based amorphous alloy can be as high as 80% while the grain size is as small as 10 nm, as seen in Fig. 4a obtained from bright-field TEM. Aside from SRO-induced nanocrystallization, it was proposed [81,82] that phase separation of a type similar to spinodal decomposition could also induce the formation of high-density nanocrystals in bulk glass formers. However, it seems that the mechanistic understanding of the phase separation-induced nanocrystallization is not clear yet. To be specific, Wang et al. [83] reported the supportive evidence through the diffraction and small angle scattering on a Zr-based bulk metallic glass, whereas Kündig et al. [84] and Wang et al. [79] reported that no phase separation could be observed until the formation of icosahedral clusters through three-dimensional atom probe tomography (3DAPT).

Different from Zr-based amorphous alloys, most Al-based amorphous alloys are a marginal glass former, which however

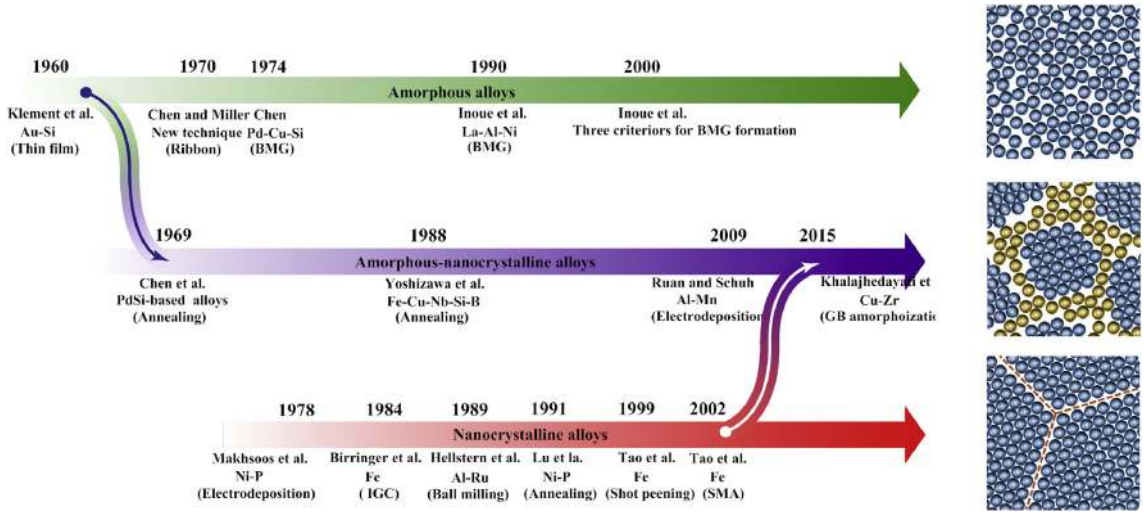

Fig. 1. Development traces of amorphous alloys, amorphous–nanocrystalline alloys, and nanocrystalline alloys.

exhibit excellent properties, such as high specific strength and good corrosion resistance. In these alloys, crystallization seems to be much easier because of the presence of quenched-in crystal nuclei [85], which in some cases manifests as a medium-range order (MRO) [86–89]. Wang et al. [85] and Bokeloh et al. [90] reported crystallization in some Al-based amorphous alloys at a temperature much lower than their crystallization temperatures, which was then attributed to the growth of the quenched-in nuclei. In the presence of a high density (10^{22}–10^{23} m^{-3}) of these pre-existing nuclei, their subsequent growth can be arrested because of the impingement of the diffusion fields that govern the crystal growth [91]. As an example, Fig. 4b obtained from dark-filed TEM shows an amorphous–nanocrystalline alloy with a high number density and small size (~16 nm) of nano-grains obtained from annealing an Al-based amorphous alloy [92].

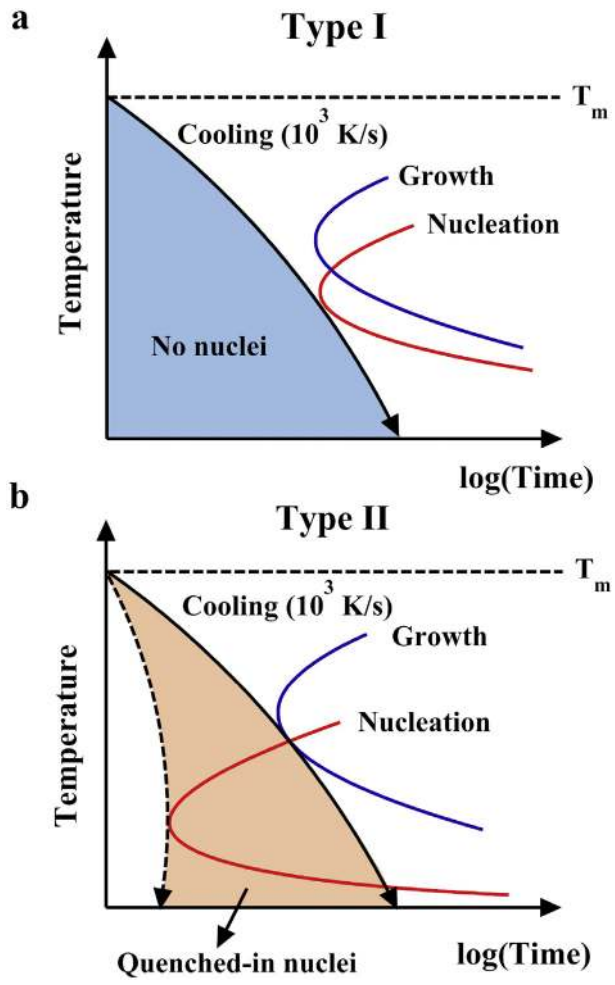

Fig. 2. Schematic illustration of (a) a good glass former without quenched-in nuclei and (b) a marginal glass former with quenched-in nuclei which cannot grow because of a kinetic barrier.

Like Al-based amorphous alloys, some Fe-based amorphous alloys, especially useful as the precursor for the fabrication of nanocrystalline soft magnetic alloys, are also a marginal glass former that can be used to make amorphous–nanocrystalline alloys. In these Fe-based amorphous alloys, Cu-centered clusters are usually needed as the active catalytic sites for the formation of the primary bcc-Fe based nanocrystals. Hono et al. [93] first investigated the formation of nanocrystals in FINEMET (FeSiBNbCu) alloy using 3DAPT. Their results showed that a high density (10^{24} m^{-3}) of Cu-clusters were formed prior to crystallization, which later served as heterogeneous nucleation sites for the primary crystallization. Pradeep et al. [94] found the similar results, as illustrated in Fig. 5a. During stage III, the large atoms of Nb can be severed as pinning sites to hinder the coarsening of bcc-Fe nanocrystals and stabilize the nanostructure. In a recent work [95], the authors found that the mechanism for stabilizing the nanostructure in the high Fe content alloys, which did contain large atoms, differed from that for the FINEMET alloys, because of the lack of hindrance from large atoms. The stabilization of nanostructure for these alloys stems from the soft-impingement effect between the shielding layers of the nanocrystals, as illustrated in Fig. 5b,c, which is similar to Al-based alloys [96].

2.2. Controlled amorphization in nanocrystalline alloys

Amorphous–nanocrystalline alloys can be also fabricated via partially transforming crystals into amorphous phases, which is known as solid-state amorphization and can be achieved through a variety of processes. These include high-energy irradiation [97], hydrogen absorption [98], annealing of diffusion couples [99], pressure-induced amorphization [100], mechanical alloying [101] and severe mechanical deformation [102]. These amorphization

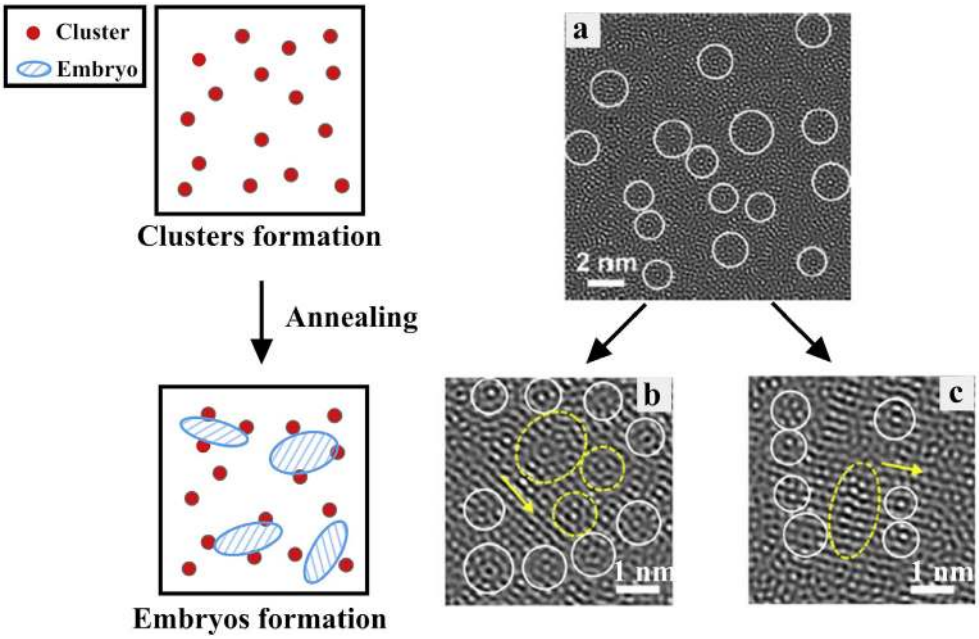

Fig. 3. Schematic drawing (left) and high-resolution TEM image (right) about the "pinning" effect of icosahedral clusters on crystallization. (Note that the TEM images are adapted from Ref. [78], reprinted with permission from Ref. [78], copyright (2011) by the American Physical Society).

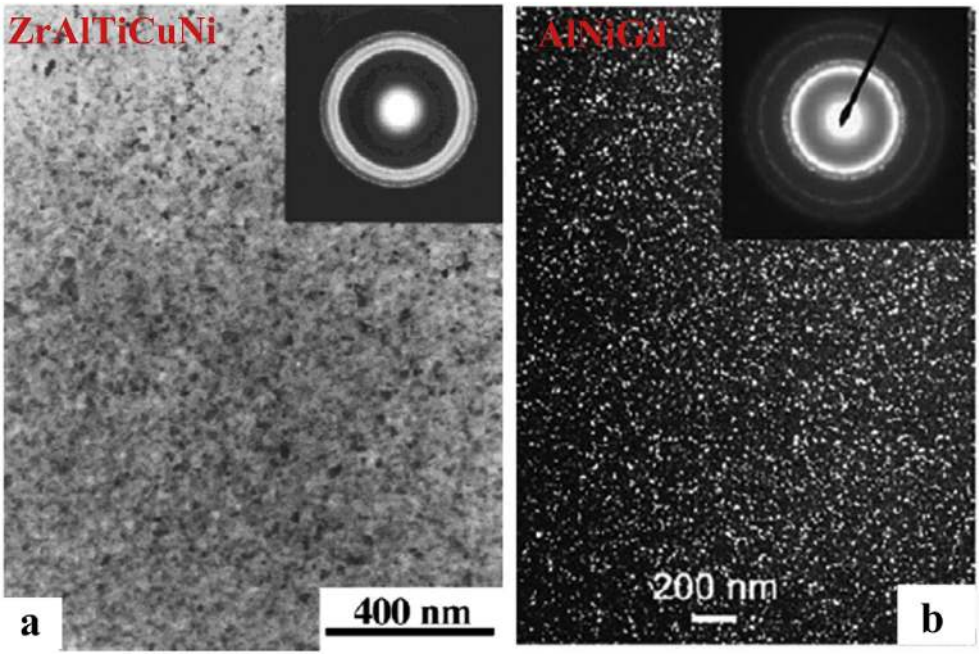

Fig. 4. TEM images of Zr-based (bright-field) and Al-based (dark-field) amorphous–nanocrystalline materials: (a) $Zr_{52.5}Al_{10}Ti_5Cu_{17.9}Ni_{14.6}$ annealed under 783 K, reprinted from Ref. [80], copyright (2000) with the permission from Cambridge University Press; (b) $Al_{90}Ni_3Gd_7$ annealed under 523 K, reprinted from Ref. [92], copyright (2005) with permission from Elsevier.

processes can be generally attributed to an increased free energy in the crystalline phase, which is higher than that of an amorphous phase [103,104]. The increase of the free energy can be caused by forming a nonequilibrium solid solution or by accumulating lattice defects [105,106]. It is interesting to note that solid-state amorphization is also possible at GBs, which results in the formation of intergranular amorphous layers [107]. Early in 1977, Clarke and Thomas [108] first observed intergranular amorphous phases in a hot-pressed ceramic. Since then, similar phenomena have been reported in several polycrystalline ceramics, such as Bi_{2O_3}-doped ZnO [109], CuO-doped TiO2 [110] and CaO-doped Al_2O_3 [111]. In the 2000s, Luo et al. [112–114] demonstrated that intergranular amorphous films could be formed at the GBs of polycrystalline alloys, such as Ni-doped W and Ni-doped Mo. The formation of such intergranular amorphous films could be associated with GB "phase" transitions, which could result from premelting, prewetting, and multilayer adsorption [115]. Interestingly, experimental results showed that there is more than one type of intergranular films [116].

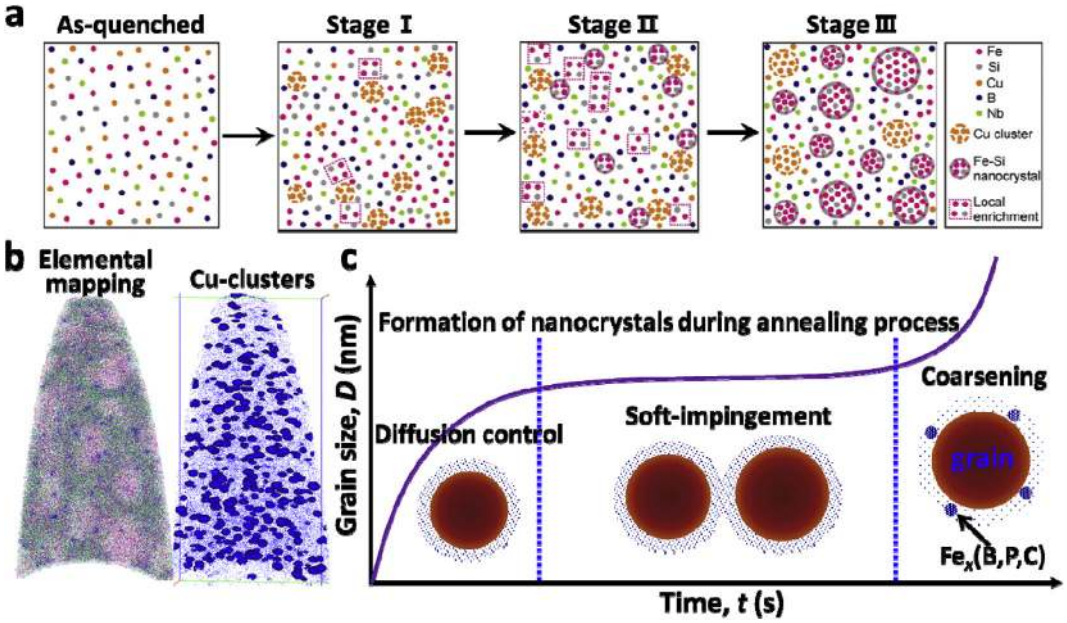

Fig. 5. (a) Schematic drawing of microstructural evolution in FINEMET alloys by primary crystallization, reprinted from Ref. [94], copyright (2014) with permission from Elsevier; (b) APT elemental map and Cu delineated by 4 at.% iso-concentration surfaces of the $Fe_{84.75}Si_2B_9P_3C_{0.5}Cu_{0.75}$ alloy after annealing at 420 °C for 48 min, reprinted with permission from Elsevier, Ref. [95] with copyright (2019); (c) illustration of the formation of nanocrystals in amorphous alloys during the isothermal annealing process.

In a much broader context, the concept of "complexion" was coined by Tang et al. [117] in 2006 to describe GBs with different characteristics, such as structural order and chemical composition. Later in 2007, Dillon et al. [116] discovered six distinct GB complexions in Al_2O_3-based ceramics (Fig. 6a). As illustrated in Fig. 6b, these GB complexions include (I) a single layer of dopants, (II) clean grain boundaries, (III) bilayers, (IV) multilayers (i.e., more than two layers), (V) intergranular film of nanoscale equilibrium thickness, and (VI) wetting films. Notably, a similar notion of "complexion" could be applied to metals [118–121]. In 2015, Khalajhedayati and Rupert [55] observed GB complexion in a nanocrystalline Cu–Zr alloy.

Since 2015, GB amorphization has been observed in a number of binary, ternary, and even multicomponent alloys, such as Ni–W [122], Cu–Zr–Hf [123] and Ni-containing high-entropy alloys (HEAs) [124]. The thickness of the intergranular amorphous films varies from 1 nm to several nanometers, as shown in Fig. 7. In these amorphous–nanocrystalline alloys, the formation of the intergranular amorphous films is mainly caused by annealing-induced solute segregation. Although GB solute segregation was first proposed by Weissmüller [125], it now becomes one of the promising routes to stabilize nanocrystalline alloys. At the fundamental level, the enhanced stability of nanocrystals could be attributed to either a reduced GB mobility due to solute drag (a kinetic mechanism) or a reduced GB energy (a thermodynamic mechanism) [37,126,127]. In 2016, Pan and Rupert [128] investigated segregation-induced GB phase transitions by using hybrid atomistic Monte Carlo/molecular dynamics simulations with Cu–Zr as the model system. They found that GBs could transition from ordered complexions (I–IV) to disordered complexions (V–VI) when the solute concentration at GBs reached a critical value. Furthermore, Schuler and Rupert [129] proposed a set of materials selection rules in 2017 to predict the formation of amorphous GB complexions. These were mainly based on two considerations, i.e., (1) encouraging the segregation of dopants to interfaces and (2) lowering the formation energy for a glassy structure. To validate their rules, a series of Cu-based binary alloys, including Cu–Zr, Cu–Hf, Cu–Nb, and Cu–Mo, were fabricated by sputtering deposition, which were subsequently heat-treated to allow for segregation and GB phase transformation. In theory, they found that the type of the GB complexion in the binary alloy can be controlled by an informed selection of the enthalpy of segregation (ΔH^{seg}) and the enthalpy of mixing (ΔH^{mix}). A positive ΔH^{seg} coupled with a negative ΔH^{mix} promotes the formation of nanoscale amorphous intergranular films, such as in Cu–Zr and Cu–Hf, whereas a positive ΔH^{seg} coupled with a positive ΔH^{mix} promotes ordered GB complexions, such as in Cu–Nb and Cu–Mo.

Aside from sputtering deposition and annealing, amorphous–nanocrystalline alloys could be also fabricated through other methods for solid-state amorphization, such as severe plastic deformation and irradiation. Early in 1993, Sundararaman [130] concluded that a nanocrystalline structure is desirable for solid-state amorphization reactions. In 2005, Ovid'ko and Sheinerman [131] developed a theoretical model to understand and predict irradiation-induced amorphization in nanocrystalline solids. They found that amorphization can be facilitated in nanocrystalline solids where the volume fraction of their interfacial phases became extremely large. However, because of the difficulty of sample fabrication, the experimental results are still limited, which warrants further research.

2.3. Controlled formation of nanostructured amorphous alloys through PVD

Apart from amorphization and crystallization from a solid precursor, PVD of thin films provides another route to synthesize nanostructured amorphous or amorphous–crystalline metals. As of today, a number of PVD methods are available and have been widely used for the fabrication of metallic thin films, including thermal evaporation [132,133], magnetron sputtering [134], pulsed laser deposition [135,136] and molecular beam epitaxy [137]. Among the above PVD methods, magnetron sputtering might be the most frequently used one because of its applicability to a wide range of chemical compositions. Compared to a liquid-to-solid

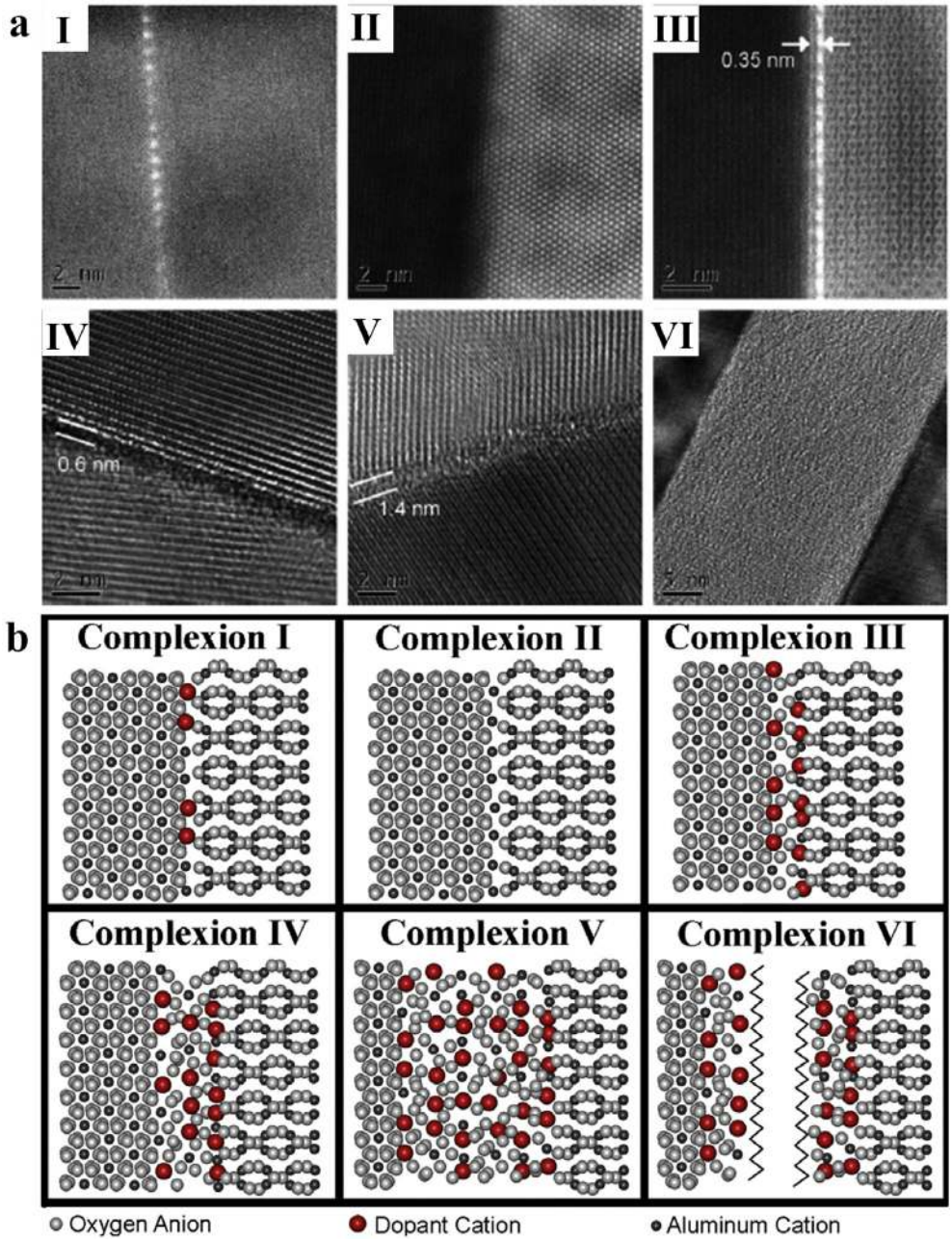

Fig. 6. (a) High-angle annular dark-field scanning transmission electron micrographs of complexions I–III, and high-resolution transmission electron micrographs of complexions IV–VI; (b) schematic of corresponding six different GB complexions: (I) a single layer of dopants, (II) clean grain boundaries, (III) bilayers, (IV) multilayers (i.e., more than two layers), (V) intergranular film of nanoscale equilibrium thickness, and (VI) wetting films. Reprinted from Ref. [116] copyright (2007) with permission from Elsevier.

melting/casting routine, a typical sputtering process entails the condensation of gaseous particles into a solid state at a cooling rate as fast as ~10^{12} K/s [138]. Aided by this, even marginal glass formers with immiscible element pairs can be synthesized into fully amorphous or crystalline–amorphous dual-phase structures via sputtering deposition [49,50,139–143].

To synthesize nanostructured amorphous–crystalline metallic films, binary alloys [49,50,139,140], HEAs [141–144], and metallic glasses doped with nitride and nitrogen [145] are promising candidate target materials. To control the chemical composition of a deposited thin film, magnetron co-sputtering [49,139–142] and reactive sputtering [143,145] were often utilized. Based on the prior works [49,50,139–143,145–147], the atomic structure of the as-deposited films strongly depends on their chemical compositions and can be tuned systematically from a crystalline to amorphous structure or to form a mixture of the two [49,50,140]. Fig. 8a–c displays the atomic structures obtained from the Al–Mo [49] binary system at different Mo contents. In this binary system, the initial increase in the atomic fraction of Mo (x_{Mo}) leads to the formation of local amorphous regions within an Al-rich crystalline matrix. As seen in Fig. 8d, a full amorphous alloy is obtained for $x_{Mo} = 32\%$, whereas a full bcc crystalline alloy is obtained for $x_{Mo} = 50\%$.

According to Inoue [14], the GFA of a binary alloy can be gaged by the mixing enthalpy (ΔH^{mix}) of the atomic pair. Usually, a good GFA corresponds to a very negative value of ΔH^{mix} and vice versa.

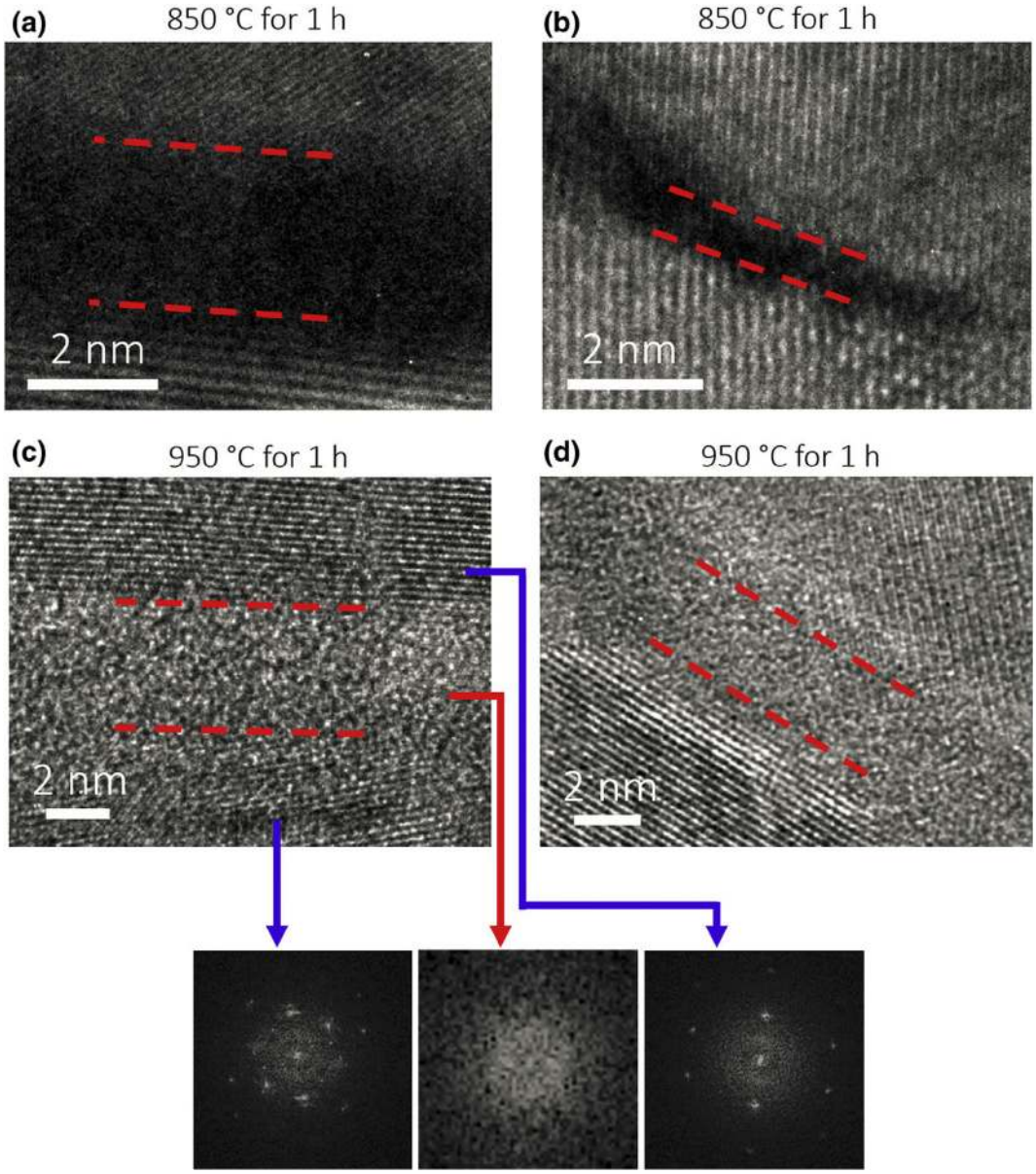

Fig. 7. High-resolution transmission electron micrograph images of amorphous intergranular films in Cu–Zr samples annealed at 850 °C and 950 °C with thickness of (a) 2.6 nm, (b) 0.8 nm, (c) 4.1 nm, and (d) 2.9 nm. Reprinted from Ref. [55] copyright (2011) with permission from Springer.

However, it can be noted that the emergence of an amorphous–crystalline composite corresponds to a slightly negative ΔH^{mix} or even positive ΔH^{mix}. In other words, the dual-phase amorphous crystalline structure is usually derived from a marginal glass former. Notably, this was already exemplified by a series of binary alloys, such as Zr–Ti ($\Delta H^{mix} = 0$ kJ/mol) [140] and Al–Mo ($\Delta H^{mix} = -5$ kJ/mol) [49]. The similar rule could be applied to ternary systems. According to Kuan et al. [147], Mg-rich nanocrystalline phases could be observed in the Zr–Cu–Mg amorphous phase, which could be attributed to the positive mixing enthalpy of Mg–Zr ($\Delta H^{mix} = +6$ kJ/mol) and the slightly negative mixing enthalpy of Mg–Cu ($\Delta H^{mix} = -3$ kJ/mol). A similar composite structure was also observed by Wu et al. [51] in the Mg–Cu–Y ternary alloy. Aside from alloying, introducing nitrogen or nitride in reactive sputtering can also facilitate the synthesis of dual-phase amorphous–crystalline nanostructures. By increasing the concentration of N_2 gas, it was observed that crystalline phases could appear in the amorphous matrix in a few alloys, such as N_2–TiVCrAlZr [143], N_2– FeCoNiCrCuAlMn [144] N_2–ZrNiAlSi [145], and N_2–ZrCu [148]. According to Chang et al. [143], nitrides can serve as the heterogeneous nucleation sites for crystallization in reactive sputtering, therefore leading to a reduced GFA.

In contrast to marginal glass formers, which form dual-phase amorphous–crystalline nanostructures in film deposition, good glass formers tend to form full nanostructured amorphous films, also termed as “nano-glass” [148–153]. Fig. 9 presents a typical nanostructured amorphous film comprised of numerous amorphous grains. In between these grains, an interface rich in free volumes was usually conceived [154]. According to the prior works [149,150], a high working pressure and a large sputtering power promote an inhomogeneous distribution of atoms and hence the formation of nano-glass, whereas a long sputtering duration causes the coarsening of amorphous grains [152]. Interestingly, apart from the chemical composition and GFA of a target, processing of the

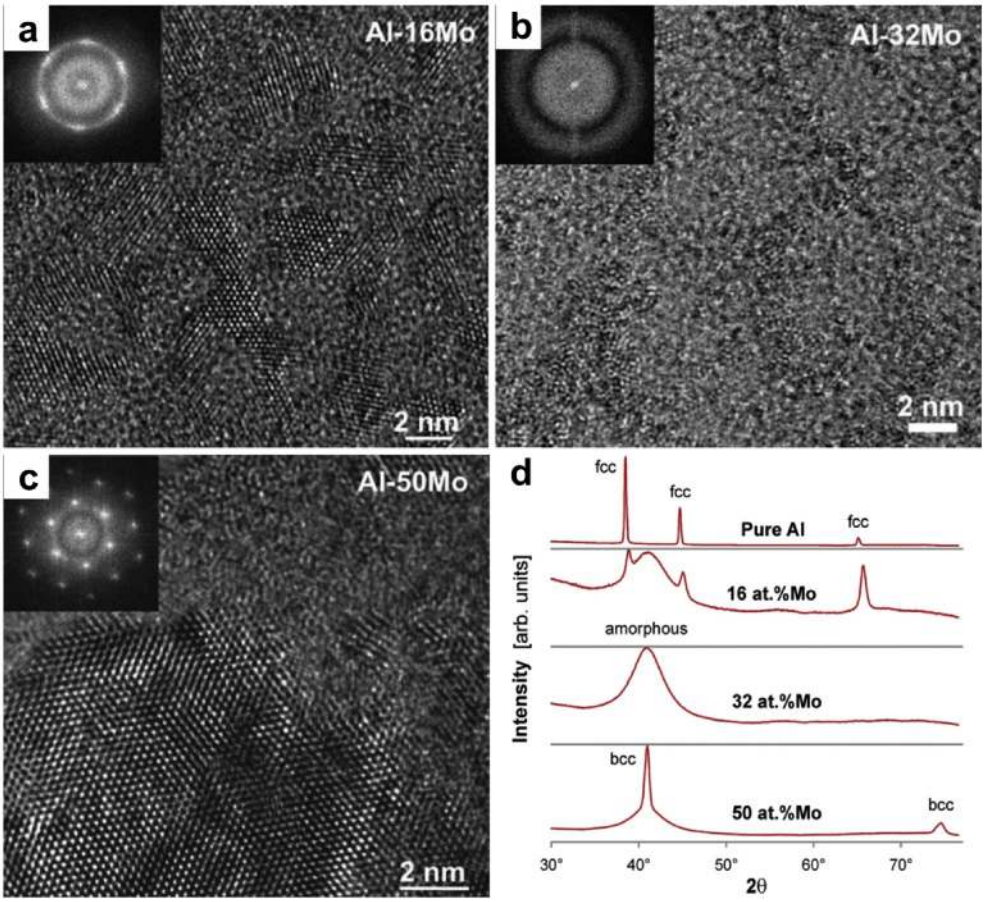

Fig. 8. (a–c) High-resolution TEM micrograph with an accompanying fast Fourier transform (TTF) inset of Al–16 at.% Mo, Al–32 at.% Mo, and Al–50 at.% Mo microstructure, respectively. (b) XRD scans of the Al–Mo films as a function of Mo content. Reprinted from Ref. [49], copyright (2011) with permission from Elsevier.

target material can also affect the formation of nano-glass [149]. As reported by Chen et al. [151], powder-compressed targets can produce a more pronounced grainy amorphous structure than targets prepared by arc melting.

3. Properties

3.1. Mechanical properties

3.1.1. Hardness and strength

Early in the 1990s, several researchers already conducted mechanical characterization of Fe- [155], Al- [156–160] and Zr-based [72,161,162] dual-phase amorphous–crystalline alloys, which were fabricated either by liquid quenching or by annealing of amorphous precursors. Their results showed that most of these alloys exhibited enhanced hardness and elastic modulus with the increasing volume fraction of nanocrystals. The strength enhancement was then attributed to the hindering of shear banding with nanocrystals [155,159,163]. Similar trends were also observed in Zr- [164] and Ti-based [165] amorphous–quasi-crystalline alloys. Apart from mechanical strengthening, mechanical softening can also occur with the presence of nanocrystals. For example, Zhang et al. [166] reported that nanocrystallization in the Zr–Cu–Fe–Al bulk amorphous alloys caused the reduction in the alloy hardness. Bi et al. [167] also observed a softening behavior in an Al-based amorphous alloy after it was cold rolled and underwent

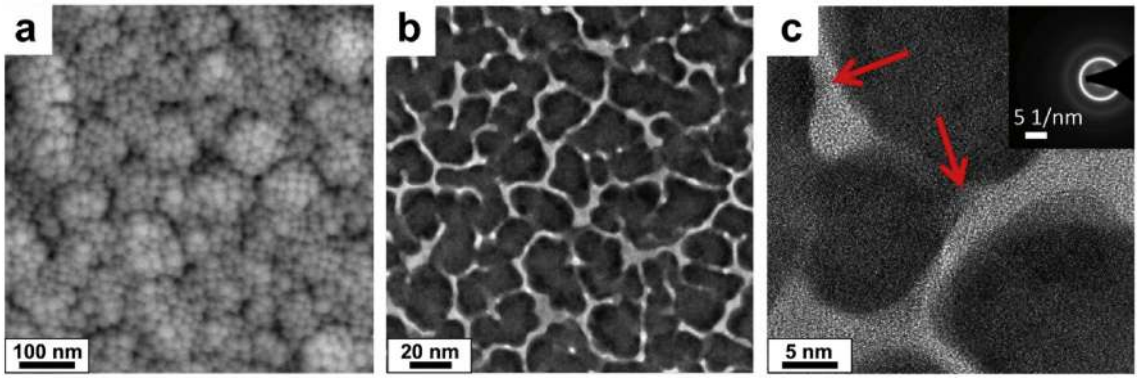

Fig. 9. (a) Cauliflower surface morphologies of the $Au_{46}Ag_6Pd_2Cu_{27}Si_{14}Al_5$ alloy obtained by SEM, reprinted from Ref. [152], copyright (2011) with permission from Elsevier. (b–c) High-resolution TEM images of $Au_{40}Cu_{28}Pd_5Ag_7Si_{20}$ alloy with FFT inset, the minor crystalline structures are pointed out by red arrows, reprinted from Ref. [150], copyright (2018) with permission from Elsevier.

polymorphic crystallization. These authors proposed that mechanical hardening, as found in the annealing-induced amorphous–nanocrystalline alloy, was due to solute enrichment in the residual amorphous matrix, whereas crystallization after cold-rolling led to softening because of the lack of solute partitioning.

In the literature, nanocrystalline alloys are known to be strong as a result of the Hall–Petch (HP) effect [168]. However, with further reduction in their grain size below a critical value, nanocrystalline alloys become softer and the so-called inverse HP effect comes into play [169], which could be attributed to the activation of GB mechanisms, such as GB sliding [170]. To mitigate this, GB doping was proposed to strengthen nanocrystalline alloys [171–175]. For example, Özerinç et al. [172] observed that the strength of the nanocrystalline Cu alloys with Nb segregation to GBs was significantly enhanced. In addition, solute segregation could also result in the formation of nanometer thick intergranular amorphous layers [55,114,129,176]. Usually, high strength is retained in the amorphous–nanocrystalline alloys obtained via GB amorphization [176].

Dual-phase amorphous–nanocrystalline alloys can also be obtained directly from PVD or electrodeposition. In 2009, Ruan and Schuh [52] measured the hardness of the Al–Mn binary alloys with the Mn content ranging from 0 to 15.8 at.%. Their results clearly showed the abrupt increase of the alloy hardness with the emergence of an amorphous phase from FCC solid solution. In 2013, Gianola et al. [177] investigated the mechanical properties of Al–Mo alloys at different Mo contents through the tensile testing of freestanding thin films. Interestingly, their results demonstrated that incorporation of Mo into Al thin films led to substantial strengthening until the formation of a two-phase FCC/amorphous mixture. The compositional dependency of the strength of the Al–Mo thin film could be well captured by a model that combines solute strengthening with GB pinning, as seen in Fig. 10. It is also interesting to note that, with further increasing Mo content beyond 20 at.%, the FCC crystals transformed to bcc, leading to a slight reduction in the tensile strength. This behavior indicated that the properties of reinforcing phase are also important to the strengthening effect of nanocrystals on the amorphous matrix. Interestingly, Zhang et al. [50] also observed GB doping in the deposited Cu–Zr film. As the Zr content increased from 0 to 8 at.% in the binary film, GB amorphization occurred, which however reduced the film strength.

3.1.2. Ductility

In 2000, Fan et al. [178] conducted a systematic study of the compressive plasticity in amorphous–nanocrystalline $Zr_{60}Cu_{20}Pd_{10}Al_{10}$ alloys prepared by thermal annealing of the corresponding amorphous precursor. These authors found that the plastic strain to failure of the alloys initially increased with the increasing volume fraction of nanocrystals, which seemingly attained a maximum value at the volume fraction of the nanocrystals ~27%. After that, further increase in the volume fraction of nanocrystals caused the reduction in the plasticity of the alloys. A similar behavior was also observed in the Cu- [179] and Ti-based [165] amorphous–nanocrystalline alloys obtained by thermal annealing. Kim and Hong [180] attributed this embrittlement observed at a high concentration of nanocrystals to the solute enrichment at the amorphous–crystalline interface. According to these authors, when a certain element reached a critical value, such as the concentration of solute Ni and Y ~20 at.% in the Al–Ni–Y alloy, fracture can be easily initiated. Recently, Li et al. [181] observed the first ductile-brittle-ductile transitions in a Fe-based amorphous–nanocrystalline alloy as the volume fraction of the Fe-based nanocrystals increased from 0 to 90%. Their results indicated that the thickness of the amorphous interface played an important role in determining the compressive plasticity of the Fe-based amorphous–nanocrystalline alloy.

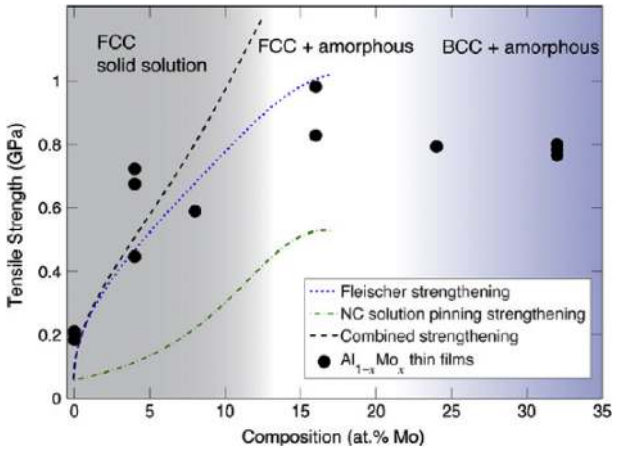

Fig. 10. Comparison of measured tensile strength of $Al_{1-x}Mo_x$ thin films with strengthening theories. Models shown include solid solution strengthening (blue curve), nanocrystalline pinning strengthening (green curve), and a combination of both (black curve). Reprinted from Ref. [177], copyright (2013) with permission from Elsevier.

Apart from thermal annealing, amorphous–nanocrystalline alloys can also be obtained by solute segregation-induced GB amorphization in nanocrystalline alloys. According to Khalajhedayati et al. [176], amorphous intergranular films at GBs act as dislocation sinks, which alleviate local stress concentration and improve plasticity. Compared to ordered interface or regular GBs in nanocrystalline alloys, which can easily fracture because of local stress concentration (Fig. 11a), the amorphous films can efficiently absorb dislocations (Fig. 11b), thereby suppressing crack nucleation and growth and improving the plasticity of the alloy, as seen in Fig. 11c,d [56,182]. Here, it may be worth mentioning that GB amorphization might deteriorate plasticity of nanocrystalline metallic films.

3.1.3. Fracture toughness

Some amorphous alloys could exhibit very high fracture toughness, such as those of Zr [183] and Pd [184]. However, Gilbert et al. [183] reported a great reduction of fracture toughness, from ~55 $MPa\sqrt{m}$ to 1 $MPa\sqrt{m}$, after thermally induced partial or full crystallization in the $Zr_{41.2}Ti_{13.8}Cu_{12.5}Ni_{10}Be_{22.5}$ (Vit 1) bulk amorphous alloy. A similar phenomenon was observed in the $La_{55}Al_{25}Cu_{10}Ni_5Co_5$ bulk amorphous alloy, which underwent a significant reduction in its impact toughness by ~90% with the presence of a small atomic percentage of crystallinity [185]. Nagendra et al. [185] related the reduction of fracture toughness to the sharp rise of relaxation times of the corresponding metallic liquid, as shown in Fig. 12. These authors suggested that densification, solute redistribution, and loss of free volume upon annealing might be responsible for the fracture toughness reduction. Ketkaew et al. [186] measured the fracture toughness of $Zr_{44}Ti_{11}Cu_{10}Ni_{10}Be_{2.5}$ and $Pd_{43}Cu2_7Ni_{10}P_{20}$, which contained a controlled volume fraction of nanocrystals after annealing. They found that the fracture toughness of the alloys decreased sharply by up to 50% when the volume fraction of the nanocrystals exceeded a critical value (~6%).

On the other hand, the fracture toughness of nanocrystalline alloys is generally low compared to that of their coarse-grained counterparts [187]. In 2001, Mirshams et al. [188] studied the fracture toughness of nanocrystalline Ni thin sheets. Their results showed that both thermal annealing and grain-boundary doping deteriorated the crack growth resistance of the nanocrystalline Ni.

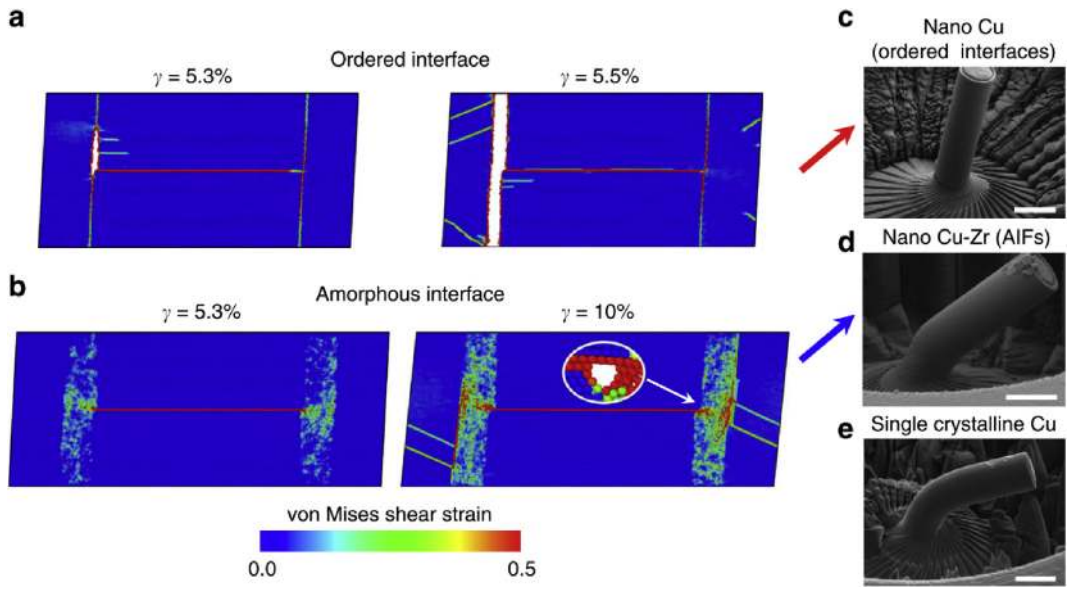

Fig. 11. Connection between interfacial structure and damage tolerance. MD simulations of dislocation absorption at (a) an ordered GB and (b) an amorphous intergranular film show the formation and propagation of crack damage. The ordered interface quickly fractures, whereas the amorphous interface diffuses the strain concentration brought by dislocation absorption and fracture is delayed. The delay of failure explains why (d) nanocrystalline Cu–Zr with amorphous intergranular films (AlFs) has ductility reminiscent of € coarse-grained Cu while retaining the high strength of (c) nanocrystalline Cu (scale bars, 5 μm). Reprinted from Ref. [176], copyright (2016) with permission from Nature Communications.

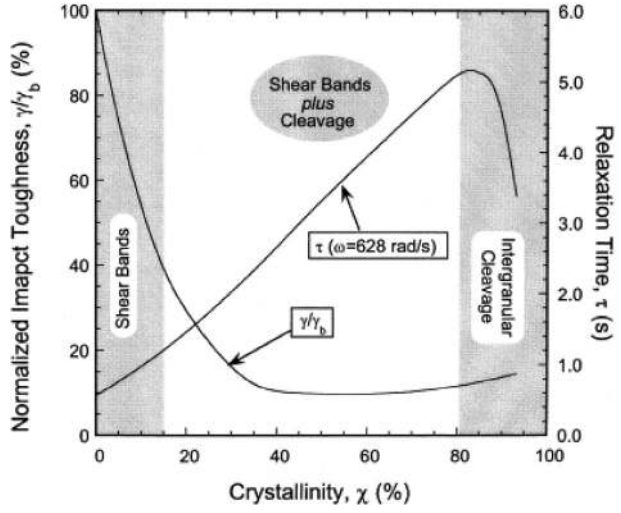

Fig. 12. Impact toughness and relaxation time as a function of material crystallinity, χ. Reprinted from Ref. [185], copyright (2000) with permission from Elsevier.

However, according to the molecular dynamics simulations of Pan and Rupert [56], once amorphous intergranular films formed at GBs, the fracture toughness of the nanocrystalline alloy might be improved as dislocations were absorbed at the amorphous–crystalline interface, leading to the retardation of crack nucleation and growth.

3.2. Functional properties

3.2.1. Soft magnetic properties

Fe-based amorphous–nanocrystalline alloys exhibit a unique combination of both high-effective permeability (μ_e) and saturation magnetization (B_s), which outperforms the variety of soft magnetic alloys [189], as shown in Fig. 13. In principle, good magnetic softness comes from low magnetic anisotropy, which is closely related to the exchange interaction of structural units [190,191]. For Fe-based amorphous–nanocrystalline alloys, their grain size is much smaller than the exchange interaction length and, thereby, the effective magnetic anisotropy will be an average over several structural units and thus reduced greatly in magnitude [192]. Meanwhile, because the B_s of α-Fe phase is much higher than that of the amorphous phase, the precipitation of α-Fe grains also gives rise to an increase in B_s of the alloy [193]. As a result, the formation of nano-sized α-Fe grains in the Fe-based amorphous alloys increases both μ_e and B_s, which helps achieving high B_s and high μ_e or the long-term goal for soft magnetic materials.

More importantly, Fe-based amorphous–nanocrystalline alloys display very low core loss (W), which is only 1/5–1/3 of that of

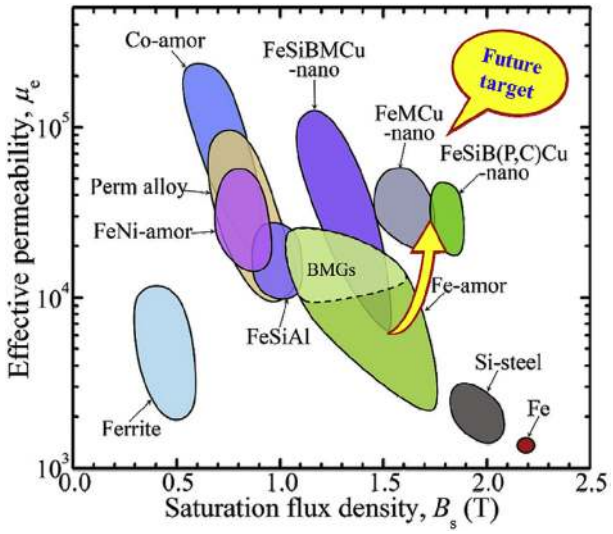

Fig. 13. Effective permeability (μ_e) at 1 kHz and saturation magnetization (B_s) for various soft magnetic materials, reprinted from Ref. [189], copyright (2016) with permission from Elsevier.

Fe–Si crystalline alloys or the so-called Si-steels, as seen in Fig. 14 [194,195]. Notably, the W of the $Fe_{85-86}Si_{1-2}B_8P_4Cu_1$ amorphous–nanocrystalline alloys is lower than that of the $Fe_{78}Si_9B_{13}$ amorphous alloys (Metglas®), the latter of which is well known to be "green materials" under high maximum magnetic induction (B_m) [196]. In addition, Fe-based amorphous–nanocrystalline alloys possess low coercivity (H_c) and near zero magnetostrictive coefficient (λ_s) [197], which makes them a promising "green material" for being used as the core material in various electronic devices [198].

3.2.2. Hydrogen storage

Mg-based amorphous–nanocrystalline alloys are a good candidate material for solid-state hydrogen storage owing to their outstanding hydrogen storage capacity, low cost, and light weight [199,200]. These dual nano-phase alloys could be easily fabricated through mechanical alloying [201,202], rapid solidification [203,204] and thermal annealing of amorphous precursors [205]. In 2005, Au [202] reported the synthesis of Mg–Ni alloys with an amorphous–nanocrystalline structure by mechanical alloying. The author found that the Mg–Ni amorphous–nanocrystalline alloys exhibited fast hydriding–dehydriding kinetics and were superior to their amorphous counterparts in hydrogen storage capacity. To be specific, the Mg 50 wt%–Ni 50 wt% amorphous–nanocrystalline alloy absorbed 5.9% hydrogen within 5 min and desorbed 5.1 wt% hydrogen within 20 min at 200 °C. As illustrated in Fig. 15, this was attributed to the unique dual nano-phase structure where the Mg matrix provides a great number of diffusion channels and interstitial sites for hydrogen migration and reaction and the Ni cluster network plays a catalytic role during the hydriding and dehydriding reaction. On the other hand, the Mg-based amorphous–nanocrystalline alloys fabricated through direct rapid solidification or subsequent devitrification of amorphous precursors also displayed promising hydrogen storage properties. For example, Kalinichenka et al. [204] studied the hydrogen storage properties of as-spun Mg–Ni–Y alloys, which consisted of Mg(Ni,Y) nanocrystals embedded in an amorphous matrix. Their results showed that these alloys can reach gravimetric hydrogen densities of up to 5.3 wt%-H with hydrogenation and dehydrogenation rates of up to 1 wt%-H/min even at the temperature of 250 °C. In 2012, Lin et al. [205] fabricated an amorphous–nanocrystalline composite by crystallizing the Mg–Ce–Ni amorphous alloy in a hydrogenation process. The composite exhibited a revisable hydrogen storage capacity of 5.3 wt% with much faster kinetics and a lower MgH_2 desorption activation energy than the original amorphous alloy.

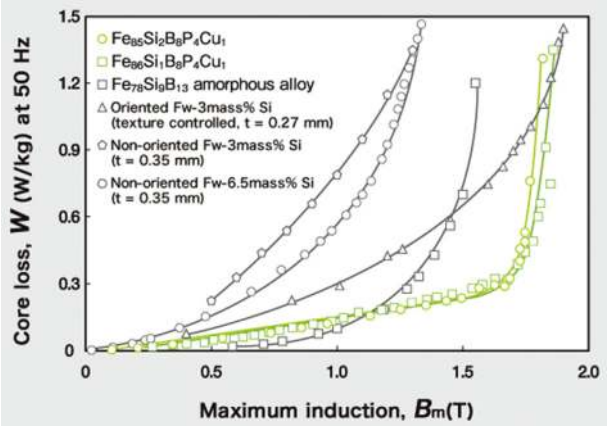

Fig. 14. Core loss (W) of $Fe_{85-86}Si_{1-2}B_8P_4Cu_1$ amorphous–nanocrystalline alloys as a function of maximum magnetic induction (B_m) at 50 Hz. The data of $Fe_{78}Si_9B_{13}$ amorphous and Fe–Si crystalline alloys are also shown for comparison, reprinted from Ref. [194], copyright (2011) with permission from Elsevier.

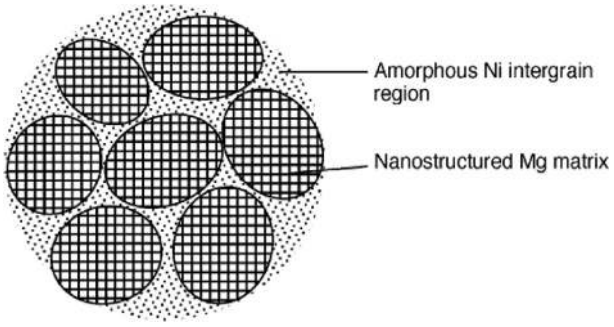

Fig. 15. Illustration of the composite structure of Mg–Ni amorphous–nanocrystalline alloy, reprinted from Ref. [202], copyright (2005) with permission from Elsevier.

3.2.3. Catalysis

Amorphous–nanocrystalline alloys could exhibit good catalytic properties, which lead to multiple applications, such as environmental remediation [206], petrochemical reaction [207] and energy conversion [3,208–215]. For example, Deng et al. [207] showed that the Ni–P amorphous–nanocrystalline alloy had a high-efficient catalytic performance on the decomposition of ammonium perchlorate, which could be used as an oxidizer in energetic composites. Pd-based amorphous–nanocrystalline alloys [213,214] also displayed a superior ethanol and methanol oxidation ability and could be considered a remarkable catalyst in direct alcohol fuel cells. In 2009, Pisarek et al. [215] developed a series of Ni–Al–Co amorphous–nanocrystalline alloys as active and selective catalysts of isophorone hydrogenation. Moreover, amorphous–nanocrystalline alloys also showed promising electrocatalytic activities for hydrogen and oxygen evolution reactions in alkaline water solutions [3,208–212,216]. For the hydrogen evolution reaction (HER), Mihailov et al. [216] reported that the amorphous–nanocrystalline Zr–Ni alloy possessed a better catalytic ability than the pure amorphous alloy with the same chemical composition. Apart from bulk amorphous–nanocrystalline alloys, nanoporous amorphous–nanocrystalline alloys can be fabricated by dealloying the corresponding amorphous precursor. These nanoporous alloys displayed superior electrocatalytic activities, which could be attributed to a high surface area and enhanced number of active sites [209,213]. On the one hand, nanocrystalline structures have a large number of low coordination atoms or active sites along the grain boundaries [3]. On the other hand, because of the lack of long-range translational ordering, amorphous structures are also rich in low-coordination sites and "defects" on their surface, facilitating adsorption, diffusion, and activation of reactants therein [208,210,216].

3.2.4. Wear resistance

In 2000, Hauert and Patscheider [217] reported that the formation of 4–7 nm sized TiC nanocrystals in the amorphous matrix of Si_3N_4 could greatly elevate the hardness of the ceramic coatings to as high as 50 GPa. Aside from the ceramic coatings, the wear resistance of amorphous–nanocrystalline alloys obtained by annealing amorphous precursors was also investigated [218,219]. For example, Gloriant [218] found that the hardness and wear resistance of a number of amorphous alloys, including ZrAlNiCu, PdNiCuP, LaAlNiCoCu bulk amorphous alloys, and AlNiY amorphous alloy ribbons, were significantly enhanced after annealing-induced nanocrystallization. Similar results were also reported by Wang et al. [219] who studied the tribological properties of the ZrAlTiCuNi bulk amorphous alloy.

Amorphous−nanocrystalline coatings could be also fabricated by several other methods, such as wire arc spraying [220], high velocity oxy fuel spraying [221], supersonic plasma spraying [222], laser cladding [223] and electrospark deposition [224]. In 2009, Cheng et al. [220] obtained a Fe-based amorphous−nanocrystalline coating on a stainless steel substrate by wire arc spraying. They found that the relative wear resistance of the coating is about three times higher than that of 3Cr13 martensitic stainless steel coatings. Additionally, Hong et al. [224] found that Zr-based amorphous−nanocrystalline coatings had good friction-reducing and anti-wear properties. Compared to the pristine alloy substrate, the frictional coefficient of the coated alloy decreased about 60% and the wear resistance increased by 57%.

4. Applications

4.1. Soft magnetism

The production of Fe-based amorphous−nanocrystalline ribbons is a very short process, which is of one step and low energy consumption. Because Fe-based amorphous−nanocrystalline ribbons are characterized by high B_s, high μ_e, low H_c, low W, and near zero λ_s, they could meet the long-term target of making strong, high efficiency, energy-saving, and quiet electronic devices [198]. In practice, Fe-based amorphous−nanocrystalline ribbons can be made into magnetic cores, such as sensors, magnetic amplifiers, high-frequency (HF) transformer and inductor cores, common mode (CM) choke cores, etc. [225−227] and used in various electronic devices in our daily life, as illustrated in Fig. 16.

Fig. 17 displays the various magnetic cores made of Fe-based amorphous−nanocrystalline soft magnetic ribbons. These HF transformer cores exhibit low core loss, high efficiency, high operation flux density, and high Curie temperature (T_c), which can reduce the transformer temperature and enable the excellent thermal stability, with the serving temperature down to −20 °C to 155 °C for a prolonged time [229]. By comparison, the high core loss in Si-steel transformers leads to a high temperature rise and results in a low conversion efficiency, which affects the electromagnetic compatibility of electronic circuits and the normal resonant working condition. For ferrite transformer cores, the main challenges are their bulk size, high temperature rise, poor resistance to unbalanced current, and large leakage at a high temperature because of their low B_s, low T_c, and low permeability below 100 kHz [230]. The current transformer includes measuring current transformer and protection current transformer. The measuring current transformer is mainly used with measuring instruments to gage the current, power, and electric energy on the line under a normal working condition. The protection current transformer is matched with relay devices, which will cut off the line in case of short-circuit or overcurrent, to protect valuable equipment in the line, such as generators and transformers. The Fe-based amorphous−nanocrystalline soft magnetic materials possess high magnetic permeability, high squareness ratio, and excellent high temperature stability, which can be applied to magnetic amplifiers to improve the output adjustment accuracy and achieve high work efficiency [231]. The power loss of copper windings for the CM chokes made of Fe-based amorphous−nanocrystalline ribbons is only 50−70% to that of ferrite, and the operation temperature is much higher than that of the ferrite chokes [232,233].

Fig. 18 illustrates the practical applications of the magnetic cores made of Fe-based amorphous−nanocrystalline soft magnetic ribbons. It was reported that the deployment of Fe-based amorphous transformers in electrical grid can save almost 70% of the potential energy loss. The no-load loss of the SH15 type amorphous distribution transformer is nearly 70% lower than that of the S11 type Si-steel transformer of the same capacity and is reduced by nearly 60% compared to the S13 type Si-steel transformer [235,236]. The CM choke cores can be applied to 500 kW and 1 MW centralized photoelectric (PV) inverters [237], as shown in Fig. 18b. The high permeability CM choke cores are suitable for the AC side electromagnetic compatibility (EMC) filtering of the high power PV inverter. The high inductance of these cores can effectively reduce the number of cores and achieve a good filtering effect. The low permeability CM choke cores are usually applied to DC side EMC filtering of a high power photovoltaic inverter. This kind of cores has good frequency characteristics, which can effectively resist unbalanced DC components and avoid burning caused by core saturation. The use of several amorphous−nanocrystalline core stacks to assemble a single choke can effectively solve the bearing current problem, which is also an effective solution to the problem of ultra-high CM noise caused by large current disturbance (peak value from tens to more than 100 amp) generated by wind power, large-range variable speed drive [238]. As shown in Fig. 18c, the Fe-based amorphous−nanocrystalline cores can be also made into direct-drive and double-fed converters covering 1 MW, 1.5 MW, 2 MW, 3 MW, etc., to be applied in wind power converters. Recently, the amorphous−nanocrystalline soft magnetic CMs have been more and more applied to an on-board charger of the battery electric vehicles and hybrid electric vehicles [238], as shown in Fig. 18d, owing to their excellent thermal stability, which can stably work over 180 °C for a long time. The wide applications of Fe-based amorphous−nanocrystalline soft magnetic materials are of great significance to the development of stronger and lighter electronic devices with a higher efficiency.

4.2. Hard magnetic materials

Early in 1995, Inoue et al. [239] found that nanostructured Fe−Nd−B alloys consisting of bcc-Fe, $Fe_{14}Nd_2B$, and an intergranular amorphous phase exhibited superior hard magnetic properties, such as a remanence (Br) of 1.28 T, a coercive field (iHc) of 252 kA/m, and a maximum energy product ((BH)max) of 146 kJ/m^3. They believed that the coexistence of the three nanoscaled ferromagnetic phases was important for the achievement of the excellent hard magnetic properties [239]. In comparison with nanocrystalline hard magnetic materials, the existence of the amorphous phase played a key role in enhancing the hard magnetic properties. On the one hand, the amorphous interphase with a thickness of 5−10 nm could act as an effective exchange magnetic coupling medium between bcc-Fe and bcc-Fe or tetragonal Fe14Nd2B phases, leading to the improved remanence [240]. On the other hand, the intergranular amorphous phase interconnected, forming a network structure that could suppress the reversion of magnetic domain walls in the central region of the otherwise soft magnetic phase, leading to the achievement of high iHc [240]. Similar notions could be also applied to the Fe−Co−Nd−Dy−B alloy. With the formation of Fe_3B, $Nd_2Fe_{14}B$, bcc-Fe in the amorphous phase under the magnetization at a field of 1256 kA/m, the remanence, intrinsic coercive force, and (BH)max of the Fe−Co−Nd−Dy−B alloy were found to be 1.6T, 1.36T, 227 kA/m, and 110 kJ/m^3, respectively [241].

4.3. Templates for porous structures

In 2017, Yu et al. [242] developed a new method to fabricate Fe-based nanoporous metallic glasses with a mean ligament size of ~75 nm and a mean pore size of ~120 nm. This was done through the selective electrochemical dissolution of the α-Fe nanocrystalline phase from a Fe−Nb−B amorphous−nanocrystalline alloy. The obtained morphology can be well controlled by controlling the

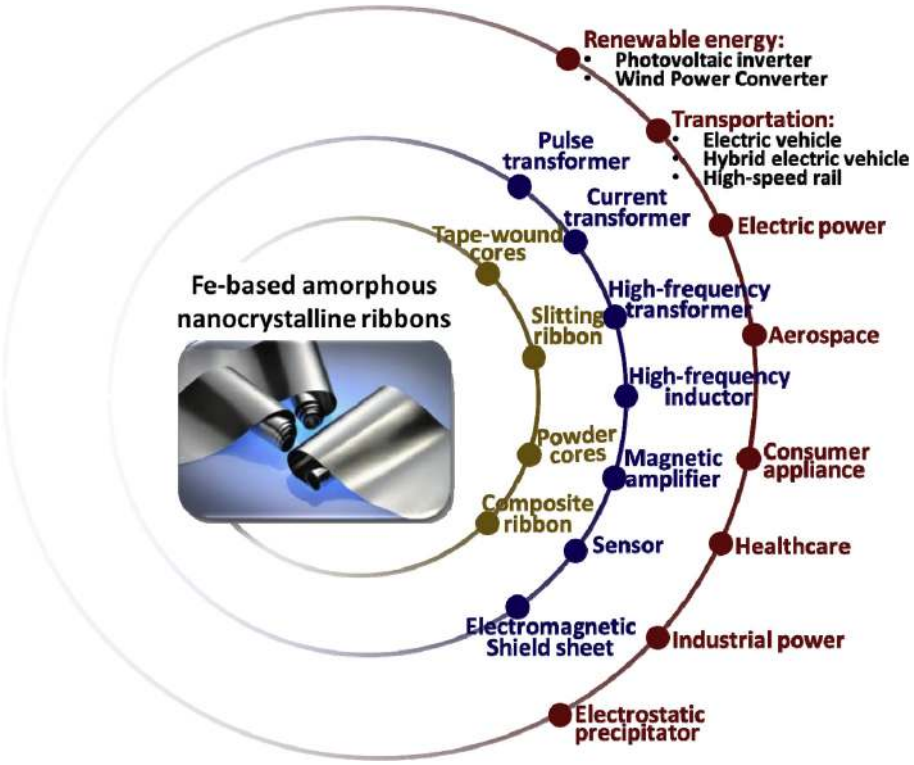

Fig. 16. Applications of amorphous–nanocrystalline soft magnetic ribbons, reprinted from Ref. [228].

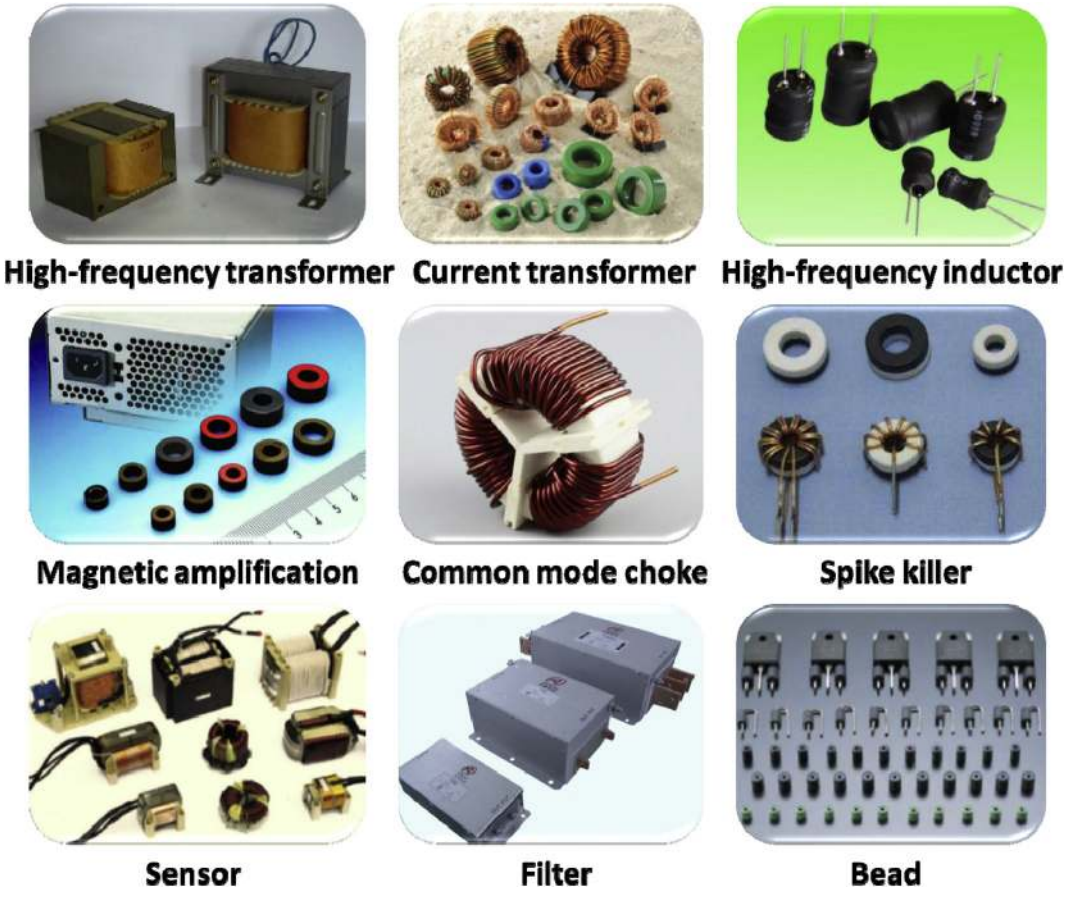

Fig. 17. Various cores made of Fe-based amorphous–nanocrystalline soft magnetic ribbons, reprinted from Ref. [234].

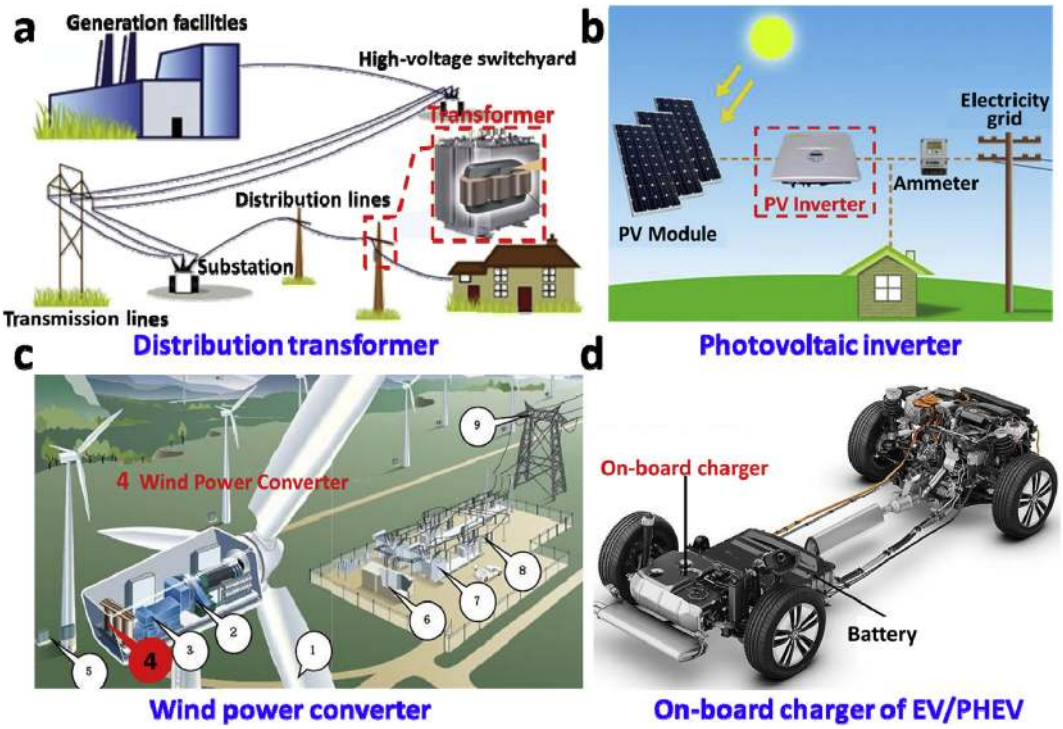

Fig. 18. (a) Distribution transformer; (b) PV inverter; (c) wind power converter, and (d) on-board charger made of amorphous–nanocrystalline soft magnetic materials, reprinted from Ref. [238].

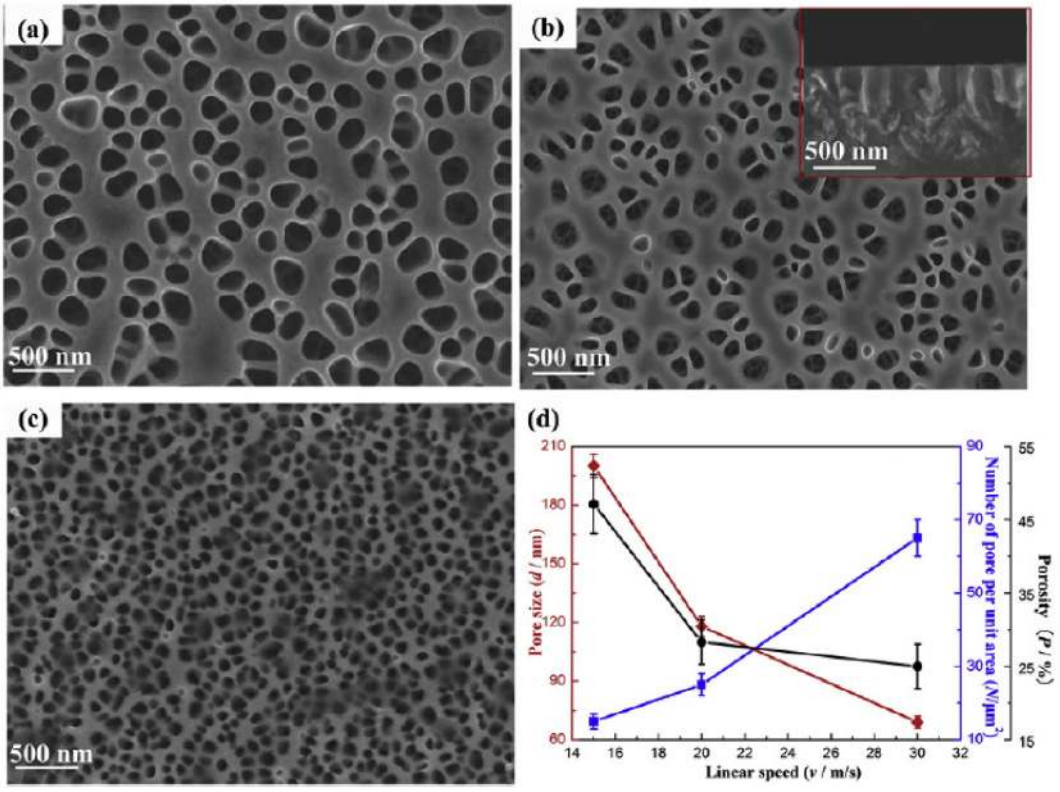

Fig. 19. SEM images of the nanoporous Fe–MGs fabricated from Fe82Nb6B12 amorphous–nanocrystalline alloy at three respective linear speeds of Cu wheel: (a)15 m/s, (b) 20 m/s (the cross-sectional view shown as inset), and (c)30 m/s. (d) Pore size, size distribution, and porosity as a function of the linear speed of Cu wheel. Reprinted from Ref. [242] copyright (2017) with permission from Elsevier.

cooling rate and/or the subsequent annealing of the amorphous alloy precursor as clearly demonstrated by Fig. 19. Similar results were also obtained on Fe–Si–B–P–Cu, Fe–B–P–Cu, and Fe–Cu–Zr–B amorphous–nanocrystalline alloys by Fu et al. [243,244] and Zhang et al. [245]. These authors argued that the preferential dissolution was triggered by the weak electrochemical stability of α-Fe nanocrystals. After removing α-Fe from the amorphous–nanocrystalline alloy, the obtained nanoporous structure possessed an ultra-large surface area, which was helpful in enhancing many chemical and physical properties for applications such as electrochemical catalysis, hydrogen storage, and reduction and oxidization reactions (Redox) in metal–air battery systems.

4.4. Corrosion protection

Some amorphous–nanocrystalline alloys, such as Al- [246–251], Fe- [252–257] and Ni-based [258–260] alloys, exhibit good corrosion resistance and can be used as the next generation corrosion resistant materials. For instance, by coating the surface of a magnesium alloy with the Al–Cu–Zn [248] and Al–Cr–Fe [247] amorphous–nanocrystalline film, Tan et al. [248] and Xu et al. [247] both found that the corrosion current of the coated magnesium alloy can be significantly reduced by two orders of magnitude in 0.6 M NaCl solution relative to the uncoated alloy. To protect 316L stainless steel, Ye et al. also developed a series of amorphous–nanocrystalline Cr–Al–Si–N films with remarkable anti-corrosion performance in seawater [246]. In addition, some Fe-based amorphous–nanocrystalline coatings were also developed, which contained a high concentration of chromium, such as Fe–Cr–B–Si–Nb–W [256], Fe–Cr–Si–B–Mn [254], and Fe–Co–Cr–Mo–C–B–Y [252]. These Fe-based amorphous–nanocrystalline coatings exhibited a higher corrosion potential and a lower corrosion current density than those of conventional hard chromium coatings and 316L stainless steel in NaCl solution.

The good anti-corrosion ability of the amorphous–nanocrystalline alloys can be partly attributed to the addition of refractory elements, such as Cr, Mo, and W, which is beneficiary to the formation of a passive film with an improved repassivation ability [253,261,262]. In addition, the partial amorphous structure of these alloys might help to mitigate the detrimental effect of microstructural heterogeneities, which are susceptible to localized corrosion attack [261,263,264]. Sweitzer et al. [249] studied the corrosion behavior of an Al-based amorphous–nanocrystalline alloy by measuring its pitting and repassivation potentials. Their results showed that the alloy possessed good resistance to the formation of micrometer-scale pits. Interestingly, Lucente and Scully [251,265] found that the pitting and alkaline corrosion behavior of Al-based amorphous–nanocrystalline alloys were comparable or even superior to those of the fully amorphous state. Johnson et al. [266] proposed that the gradient compositional field in the amorphous matrix was able to provide highly corrosion resistant zones around solute-lean precipitates, thereby resulting in excellent corrosion resistance.

5. Summary

To summarize, we may categorize the amorphous–nanocrystalline alloys hitherto reported into three types, being in line with the different fabrication or synthesis methods:

(1) The amorphous–nanocrystalline alloys obtained through the controlled nanocrystallization in amorphous alloy “templates”. Notably, many amorphous alloys are able to act as the templates or precursors to form amorphous–nanocrystalline alloys, including the good glass forming systems, such as Zr-based bulk amorphous alloys [72], and the marginal glass forming systems, such as Al- [160] and Fe-based [47] amorphous alloys. With the precipitation of nanocrystals from an amorphous matrix, the hardness and strength of the amorphous–nanocrystalline alloys so obtained could be enhanced but their ductility and fracture toughness generally deteriorate. On the other hand, compared to the original amorphous alloy, some functional properties of the amorphous–nanocrystalline alloys could be greatly improved, such as their magnetic properties.

(2) The amorphous–nanocrystalline alloys obtained through GB amorphization in nanocrystalline alloys. Up to now, GB amorphization was observed only in a few binary/ternary systems, such as Cu–Zr [55] and Cu–Zr-Hf [123]. With the replacement of grain boundaries by amorphous intergranular films, both ductility and fracture toughness of the amorphous–nanocrystalline alloy could be greatly improved without jeopardizing the strength of the original nanocrystalline alloy.

(3) The amorphous–nanocrystalline thin films obtained through PVD. Because PVD entails a high cooling rate (~10^{12} K/s), amorphous–nanocrystalline films can be obtained even from poor glass formers. Therefore, binary alloys [49,50,139,140], HEAs [141–144], and amorphous alloys doped with nitride and nitrogen [145] are all promising candidate systems for making amorphous–nanocrystalline thin films. These films could exhibit superior functional/structural properties, such as excellent wear and corrosion resistance.

Owing to the unique combination of structural/functional properties, we have seen the use of amorphous–nanocrystalline alloys in a variety of applications, as a soft or hard magnetic material for energy-related applications, as a hydrogen storage material, as a template for generating porous nanostructures for electrochemical catalysis, or as anti-wear and anti-corrosion films for surface protection. As the research of amorphous–nanocrystalline alloys continues to fruition, we expect more interesting properties and exciting applications from this type of alloys to be reported in near future.

Declaration of competing interest

The authors declare that they have no known competing financial interests or personal relationships that could have appeared to influence the work reported in this paper.

Acknowledgments

The research of YY is supported by the Research Grants Council (RGC), the Hong Kong government through the General Research Fund (GRF) with the grant number CityU11200719 and CityU11213118.

References

[1] H. Gleiter, in: Nanocrystalline Materials. Progress in Materials Science, vol. 33, Elsevier, 1989, pp. 223–315.
[2] C. Suryanarayana, C. Koch, Nanocrystalline materials–Current research and future directions, Hyperfine Interact. 130 (2000) 5.
[3] M. Trudeau, J. Ying, Nanocrystalline materials in catalysis and electrocatalysis: structure tailoring and surface reactivity, Nanostructured Mater. 7 (1996) 245–258.
[4] K. Kumar, H. Van Swygenhoven, S. Suresh, Mechanical behavior of nanocrystalline metals and alloys, Acta Mater. 51 (2003) 5743–5774.
[5] W.K. Jun, R. Willens, P. Duwez, Non-crystalline structure in solidified gold–silicon alloys, Nature 187 (1960) 869.
[6] B. Bagley, H. Chen, D. Turnbull, Characterization of amorphous alloy films, Mater. Res. Bull. 3 (1968) 159–168.

[7] C. Tsuei, Electrical resistance and thermoelectric power of an amorphous Te 70 Cu 25 Au 5 alloy, Phys. Rev. 170 (1968) 775.
[8] H. Chen, D. Turnbull, Evidence of a glass–liquid transition in a gold–germanium–silicon alloy, J. Chem. Phys. 48 (1968) 2560–2571.
[9] H. Chen, C. Miller, A rapid quenching technique for the preparation of thin uniform films of amorphous solids, Rev. Sci. Instrum. 41 (1970) 1237–1238.
[10] E. Babic, E. Girt, R. Krsnik, B. Leontic, Production of large samples of ultra-rapidly quenched alloys of aluminium by means of a rotating mill device, J. Phys. E Sci. Instrum. 3 (1970) 1014.
[11] D. Turnbull, Under what conditions can a glass be formed? Contemp. Phys. 10 (1969) 473–488.
[12] A. Inoue, T. Zhang, T. Masumoto, Glass-forming ability of alloys, J. Non-Cryst. Solids 156 (1993) 473–480.
[13] W.L. Johnson, Bulk glass-forming metallic alloys: science and technology, MRS Bull. 24 (1999) 42–56.
[14] A. Inoue, Stabilization of metallic supercooled liquid and bulk amorphous alloys, Acta Mater. 48 (2000) 279–306.
[15] A. Inoue, T. Zhang, T. Masumoto, Zr–Al–Ni amorphous alloys with high glass transition temperature and significant supercooled liquid region, Mater. Trans., JIM 31 (1990) 177–183.
[16] T. Zhang, A. Inoue, T. Masumoto, Amorphous Zr–Al–TM (TM= Co, Ni, Cu) alloys with significant supercooled liquid region of over 100 K, Mater. Trans., JIM 32 (1991) 1005–1010.
[17] A. Inoue, K. Ohtera, K. Kita, T. Masumoto, New amorphous Mg-Ce-Ni alloys with high strength and good ductility, Jpn. J. Appl. Phys. 27 (1988) L2248.
[18] A. Inoue, T. Zhang, T. Masumoto, Al–La–Ni amorphous alloys with a wide supercooled liquid region, Mater. Trans., JIM 30 (1989) 965–972.
[19] T. Zhang, A. Inoue, Thermal and mechanical properties of Ti–Ni–Cu–Sn amorphous alloys with a wide supercooled liquid region before crystallization, Mater. Trans., JIM 39 (1998) 1001–1006.
[20] A. Inoue, J.S. Gook, Fe-based ferromagnetic glassy alloys with wide supercooled liquid region, Mater. Trans., JIM 36 (1995) 1180–1183.
[21] A. Inoue, A. Katsuya, Multicomponent Co-based amorphous alloys with wide supercooled liquid region, Mater. Trans., JIM 37 (1996) 1332–1336.
[22] R. Akatsuka, T. Zhang, H. Koshiba, A. Inoue, Preparation of new Ni-based amorphous alloys with a large supercooled liquid region, Mater. Trans., JIM 40 (1999) 258–261.
[23] A. Peker, W.L. Johnson, A highly processable metallic glass: Zr41. 2Ti13. 8Cu12. 5Ni10. 0Be22. 5, Appl. Phys. Lett. 63 (1993) 2342–2344.
[24] A. Inoue, T. Zhang, N. Nishiyama, K. Ohba, T. Masumoto, Preparation of 16 mm diameter rod of amorphous Zr65Al7. 5Ni10Cu17. 5 alloy, Mater. Trans., JIM 34 (1993) 1234–1237.
[25] A. Inoue, T. Zhang, T. Masumoto, Production of amorphous cylinder and sheet of La55Al25Ni20 alloy by a metallic mold casting method, Mater. Trans., JIM 31 (1990) 425–428.
[26] M. Ashby, A. Greer, Metallic glasses as structural materials, Scr. Mater. 54 (2006) 321–326.
[27] A.L. Greer, Y.Q. Cheng, E. Ma, Shear bands in metallic glasses, Mater. Sci. Eng. R Rep. 74 (2013) 71–132.
[28] Y.C. Hu, Y.Z. Wang, R. Su, C.R. Cao, F. Li, C.W. Sun, Y. Yang, P.F. Guan, D.W. Ding, Z.L. Wang, A highly efficient and self-stabilizing metallic-glass catalyst for electrochemical hydrogen generation, Adv. Mater. 28 (2016) 10293–10297.
[29] J.Q. Wang, Y.H. Liu, M.W. Chen, G.Q. Xie, D.V. Louzguine-Luzgin, A. Inoue, J.H. Perepezko, Rapid degradation of azo dye by Fe-based metallic glass powder, Adv. Funct. Mater. 22 (2012) 2567–2570.
[30] R. Birringer, H. Gleiter, H.-P. Klein, P. Marquardt, Nanocrystalline materials an approach to a novel solid structure with gas-like disorder? Phys. Lett. A 102 (1984) 365–369.
[31] E. Hellstern, H.J. Fecht, Z. Fu, W. Johnson, Structural and thermodynamic properties of heavily mechanically deformed Ru and AlRu, J. Appl. Phys. 65 (1989) 305–310.
[32] K. Lu, J. Wang, W. Wei, A new method for synthesizing nanocrystalline alloys, J. Appl. Phys. 69 (1991) 522–524.
[33] N. Tao, M. Sui, J. Lu, K. Lua, Surface nanocrystallization of iron induced by ultrasonic shot peening, Nanostructured Mater. 11 (1999) 433–440.
[34] N. Tao, Z. Wang, W. Tong, M. Sui, J. Lu, K. Lu, An investigation of surface nanocrystallization mechanism in Fe induced by surface mechanical attrition treatment, Acta Mater. 50 (2002) 4603–4616.
[35] U. Erb, A.M. El-Sherik, G. Palumbo, K.T. Aust, Synthesis, structure and properties of electroplated nanocrystalline materials, Nanostructured Mater. 2 (1993) 383–390.
[36] S. Tjong, H. Chen, Nanocrystalline materials and coatings, Mater. Sci. Eng. R Rep. 45 (2004) 1–88.
[37] H.R. Peng, M.M. Gong, Y.Z. Chen, F. Liu, Thermal stability of nanocrystalline materials: thermodynamics and kinetics, Int. Mater. Rev. 62 (2017) 303–333.
[38] G. Higgins, Grain-boundary migration and grain growth, Met. Sci. 8 (1974) 143–150.
[39] M.A. Meyers, A. Mishra, D.J. Benson, Mechanical properties of nanocrystalline materials, Prog. Mater. Sci. 51 (2006) 427–556.
[40] P. Rastogi, P. Duwez, Rate of crystallization of an amorphous Fe-P-C alloy, J. Non-Cryst. Solids 5 (1970) 1–16.
[41] P. Duhaj, D. Barančok, A. Ondrejka, The study of transformation kinetics of the amorphous Pd-Si alloys, J. Non-Cryst. Solids 21 (1976) 411–428.
[42] T. Masumoto, Y. Waseda, H. Kimura, A. Inoue, Thermal instability and crystallization characteristics of amorphous metal-metalloid system, Sci. Rep. Res. Inst. Tohoku Univ. Ser. A Phys. Chem. Metall. 26 (1976) 21–35.
[43] P. Gaskell, D.J. Smith, Investigations of the structure of amorphous and partially crystalline metallic alloys by high resolution electron microscopy, J. Microsc. 119 (1980) 63–72.
[44] R. Diegle, J. Slater, Influence of crystallinity on corrosion behavior of ferrous alloys, Corrosion 32 (1976) 155–157.
[45] E. Wohlfarth, Magnetic properties of crystalline and amorphous alloys: a systematic discussion based on the Rhodes-Wohlfarth plot, J. Magn. Magn. Mater. 7 (1978) 113–120.
[46] A. Inoue, S. Sakai, H. Kimura, T. Masumoto, Crystallization temperature and hardness of new chromium-based amorphous alloys, Trans. Japan Inst. Metals 20 (1979) 255–262.
[47] Y. Yoshizawa, S. Oguma, K. Yamauchi, New Fe-based soft magnetic alloys composed of ultrafine grain structure, J. Appl. Phys. 64 (1988) 6044–6046.
[48] E. Vafaei-Makhsoos, E.L. Thomas, L.E. Toth, Electron microscopy of crystalline and amorphous Ni-P electrodeposited films: in-situ crystallization of an amorphous solid, Metal. Trans. A 9 (1978) 1449–1460.
[49] C. Ophus, E. Luber, M. Edelen, Z. Lee, L. Fischer, S. Evoy, D. Lewis, U. Dahmen, V. Radmilovic, D. Mitlin, Nanocrystalline–amorphous transitions in Al–Mo thin films: bulk and surface evolution, Acta Mater. 57 (2009) 4296–4303.
[50] P. Zhang, J.Y. Zhang, J. Li, G. Liu, K. Wu, Y.Q. Wang, J. Sun, Microstructural evolution, mechanical properties and deformation mechanisms of nanocrystalline Cu thin films alloyed with Zr, Acta Mater. 76 (2014) 221–237.
[51] G. Wu, K.-C. Chan, L. Zhu, L. Sun, J. Lu, Dual-phase nanostructuring as a route to high-strength magnesium alloys, Nature 545 (2017) 80.
[52] S. Ruan, C.A. Schuh, Electrodeposited Al–Mn alloys with microcrystalline, nanocrystalline, amorphous and nano-quasicrystalline structures, Acta Mater. 57 (2009) 3810–3822.
[53] H. Cesiulis, A. Baltutiene, M. Donten, Z. Stojek, Increase in rate of electrodeposition and in Ni (II) concentration in the bath as a way to control grain size of amorphous/nanocrystalline Ni-W alloys, J. Solid State Electrochem. 6 (2002) 237–244.
[54] C. Ophus, N. Nelson Fitzpatrick, Z. Lee, E. Luber, C. Harrower, K. Westra, U. Dahmen, V. Radmilovic, S. Evoy, D. Mitlin, Resonance properties and microstructure of ultracompliant metallic nanoelectromechanical systems resonators synthesized from Al–32 at.% Mo amorphous-nanocrystalline metallic composites, Appl. Phys. Lett. 92 (2008) 123108.
[55] A. Khalajhedayati, T.J. Rupert, High-temperature stability and grain boundary complexion formation in a nanocrystalline Cu-Zr alloy, JOM 67 (2015) 2788–2801.
[56] Z. Pan, T.J. Rupert, Amorphous intergranular films as toughening structural features, Acta Mater. 89 (2015) 205–214.
[57] R. Kirchheim, Grain coarsening inhibited by solute segregation, Acta Mater. 50 (2002) 413–419.
[58] H. Chen, D. Turnbull, Formation, stability and structure of palladium-silicon based alloy glasses, Acta Metall. 17 (1969) 1021–1031.
[59] T. Kulik, T. Horubał, H. Matyja, Flash annealing nanocrystallization of Fe-Si-B-based glasses, Mater. Sci. Eng.: A 157 (1992) 107–112.
[60] R. Nicula, M. Stir, K. Ishizaki, J.-M. Català-Civera, S. Vaucher, Rapid nanocrystallization of soft-magnetic amorphous alloys using microwave induction heating, Scr. Mater. 60 (2009) 120–123.
[61] N. Boucharat, R. Hebert, H. Rösner, R. Valiev, G. Wilde, Nanocrystallization of amorphous Al88Y7Fe5 alloy induced by plastic deformation, Scr. Mater. 53 (2005) 823–828.
[62] R. Hebert, J. Perepezko, Effect of cold-rolling on the crystallization behavior of amorphous Al88Y7Fe5 alloy, Mater. Sci. Eng.: A 375 (2004) 728–732.
[63] J. Fan, A. Chen, M. Fu, J. Lu, A novel structural gradient metallic glass composite with enhanced mechanical properties, Scr. Mater. 61 (2009) 608–611.
[64] Q. Wang, Y. Yang, H. Jiang, C. Liu, H. Ruan, J. Lu, Superior tensile ductility in bulk metallic glass with gradient amorphous structure, Sci. Rep. 4 (2014) 4757.
[65] Y. He, G. Shiflet, S. Poon, Ball milling-induced nanocrystal formation in aluminum-based metallic glasses, Acta Metall. Mater. 43 (1995) 83–91.
[66] W. Qin, T. Nagase, Y. Umakoshi, Electron irradiation-induced nanocrystallization of amorphous Fe85B15 alloy: evidence for athermal nature, Acta Mater. 57 (2009) 1300–1307.
[67] T. Nagase, Y. Umakoshi, Phase stability of amorphous and crystalline phases in melt-spun Zr66. 7Cu33. 3 alloy under electron irradiation, Scr. Mater. 48 (2003) 1237–1242.
[68] L. Shao, B.P. Gorman, A. Aitkaliyeva, N. David Theodore, G. Xie, Nanometer-scale tunnel formation in metallic glass by helium ion irradiation, Appl. Phys. Lett. 101 (2012), 041901.
[69] A. Sypień, J. Kusiński, G.J. Kusiński, E.C. Nelson, TEM studies of the FeSiB amorphous alloy nanocrystallized by means of Nd: YAG-pulsed laser heating, Mater. Chem. Phys. 81 (2003) 390–392.
[70] T. Ichitsubo, E. Matsubara, T. Yamamoto, H. Chen, N. Nishiyama, J. Saida, K. Anazawa, Microstructure of fragile metallic glasses inferred from ultrasound-accelerated crystallization in Pd-based metallic glasses, Phys. Rev. Lett. 95 (2005) 245501.
[71] W.-H. Wang, C. Dong, C. Shek, Bulk metallic glasses, Mater. Sci. Eng. R Rep. 44 (2004) 45–89.

[72] A. Inoue, C. Fan, J. Saida, T. Zhang, High-strength Zr-based bulk amorphous alloys containing nanocrystalline and nanoquasicrystalline particles, Sci. Technol. Adv. Mater. 1 (2000) 73–86.
[73] G. Wilde, N. Boucharat, R.J. Hebert, H. Rösner, W.S. Tong, J.H. Perepezko. Nanocrystallization in Al-rich metallic glasses, Adv. Eng. Mater. 5 (2003) 125–130.
[74] J.H. Perepezko, R.J. Hebert, Amorphous aluminum alloys—synthesis and stability, JOM 54 (2002) 34–39.
[75] L. Xing, T. Hufnagel, J. Eckert, W. Löser, L. Schultz, Relation between short-range order and crystallization behavior in Zr-based amorphous alloys, Appl. Phys. Lett. 77 (2000) 1970–1972.
[76] C. Fan, M. Imafuku, H. Kurokawa, A. Inoue, V. Haas, Investigation of short-range order in nanocrystal-forming Zr 60 Cu 20 Pd 10 Al 10 metallic glass and the mechanism of nanocrystal formation, Appl. Phys. Lett. 79 (2001) 1792–1794.
[77] C. Fan, A. Inoue, Influence of the liquid states on the crystallization process of nanocrystal-forming Zr–Cu–Pd–Al metallic glasses, Appl. Phys. Lett. 75 (1999) 3644–3646.
[78] Q. Wang, C.T. Liu, Y. Yang, Y. Dong, J. Lu, Atomic-scale structural evolution and stability of supercooled liquid of a Zr-based bulk metallic glass, Phys. Rev. Lett. 106 (2011) 215505.
[79] Z. Wang, S. Ketov, C. Chen, Y. Shen, Y. Ikuhara, A. Tsarkov, D. Louzguine-Luzgin, J. Perepezko, Nucleation and thermal stability of an icosahedral nanophase during the early crystallization stage in Zr-Co-Cu-Al metallic glasses, Acta Mater. 132 (2017) 298–306.
[80] J. Wang, B. Choi, T. Nieh, C. Liu, Crystallization and nanoindentation behavior of a bulk Zr–Al–Ti–Cu–Ni amorphous alloy, J. Mater. Res. 15 (2000) 798–807.
[81] S. Schneider, P. Thiyagarajan, W. Johnson, Formation of nanocrystals based on decomposition in the amorphous Zr41. 2Ti13. 8Cu12. 5Ni10Be22. 5 alloy, Appl. Phys. Lett. 68 (1996) 493–495.
[82] W.-H. Wang, Q. Wei, S. Friedrich, Microstructure, decomposition, and crystallization in Zr 41 Ti 14 Cu 12.5 Ni 10 Be 22.5 bulk metallic glass, Phys. Rev. B 57 (1998) 8211.
[83] X.-L. Wang, J. Almer, C. Liu, Y. Wang, J. Zhao, A. Stoica, D. Haeffner, W. Wang, In situ synchrotron study of phase transformation behaviors in bulk metallic glass by simultaneous diffraction and small angle scattering, Phys. Rev. Lett. 91 (2003) 265501.
[84] A. Kündig, M. Ohnuma, T. Ohkubo, K. Hono, Early crystallization stages in a Zr–Cu–Ni–Al–Ti metallic glass, Acta Mater. 53 (2005) 2091–2099.
[85] J. Wang, H. Zhang, X. Gu, K. Lu, F. Sommer, E. Mittemeijer, Identification of nanocrystal nucleation and growth in Al 85 Ni 5 Y 8 Co 2 metallic glass with quenched-in nuclei, Appl. Phys. Lett. 80 (2002) 3319–3321.
[86] H. Sheng, Y. Cheng, P. Lee, S. Shastri, E. Ma, Atomic packing in multicomponent aluminum-based metallic glasses, Acta Mater. 56 (2008) 6264–6272.
[87] Y. Kalay, I. Kalay, J. Hwang, P. Voyles, M. Kramer, Local chemical and topological order in Al–Tb and its role in controlling nanocrystal formation, Acta Mater. 60 (2012) 994–1003.
[88] N. Wu, M. Yan, L. Zuo, J. Wang, Correlation between medium-range order structure and glass-forming ability for Al-based metallic glasses, J. Appl. Phys. 115 (2014), 043523.
[89] D. Miracle, O. Senkov, A geometric model for atomic configurations in amorphous Al alloys, J. Non-Cryst. Solids 319 (2003) 174–191.
[90] J. Bokeloh, N. Boucharat, H. Rösner, G. Wilde, Primary crystallization in Al-rich metallic glasses at unusually low temperatures, Acta Mater. 58 (2010) 3919–3926.
[91] D. Allen, J. Foley, J. Perepezko, Nanocrystal development during primary crystallization of amorphous alloys, Acta Mater. 46 (1998) 431–440.
[92] M.C. Gao, G. Shiflet, Devitrification sequence map in the glass forming Al–Ni–Gd system, Scr. Mater. 53 (2005) 1129–1134.
[93] K. Hono, D. Ping, M. Ohnuma, H. Onodera, Cu clustering and Si partitioning in the early crystallization stage of an Fe73. 5Si13. 5B9Nb3Cu1 amorphous alloy, Acta Mater. 47 (1999) 997–1006.
[94] K.G. Pradeep, G. Herzer, P. Choi, D. Raabe, Atom probe tomography study of ultrahigh nanocrystallization rates in FeSiNbBCu soft magnetic amorphous alloys on rapid annealing, Acta Mater. 68 (2014) 295–309.
[95] T. Liu, F. Li, A. Wang, L. Xie, Q. He, J. Luan, A. He, X. Wang, C. Liu, Y. Yang, High performance Fe-based nanocrystalline alloys with excellent thermal stability, J. Alloy. Comp. 776 (2019) 606–613.
[96] M.T. Clavaguera-Mora, N. Clavaguera, D. Crespo, T. Pradell, Crystallisation kinetics and microstructure development in metallic systems, Prog. Mater. Sci. 47 (2002) 559–619.
[97] A.T. Motta, Amorphization of intermetallic compounds under irradiation—a review, J. Nucl. Mater. 244 (1997) 227–250.
[98] K. Aoki, T. Masumoto, Solid state amorphization of intermetallic compounds by hydrogenation, J. Alloy. Comp. 194 (1993) 251–261.
[99] R. Schwarz, W. Johnson, Formation of an amorphous alloy by solid-state reaction of the pure polycrystalline metals, Phys. Rev. Lett. 51 (1983) 415.
[100] S.M. Sharma, S. Sikka, Pressure induced amorphization of materials, Prog. Mater. Sci. 40 (1996) 1–77.
[101] B. Murty, M.M. Rao, S. Ranganathan, Milling maps and amorphization during mechanical alloying, Acta Metall. Mater. 43 (1995) 2443–2450.
[102] J. Huang, Y. Zhu, X. Liao, R. Valiev, Amorphization of TiNi induced by high-pressure torsion, Philos. Mag. Lett. 84 (2004) 183–190.
[103] D. Wolf, P. Okamoto, S. Yip, J. Lutsko, M. Kluge, Thermodynamic parallels between solid-state amorphization and melting, J. Mater. Res. 5 (1990) 286–301.
[104] W.L. Johnson, Thermodynamic and kinetic aspects of the crystal to glass transformation in metallic materials, Prog. Mater. Sci. 30 (1986) 81–134.
[105] J. Koike, Elastic instability of crystals caused by static atom displacement: a mechanism for solid-state amorphization, Phys. Rev. B 47 (1993) 7700.
[106] H. Fecht, Defect-induced melting and solid-state amorphization, Nature 356 (1992) 133.
[107] I.A. Ovid'ko, A.B. Reizis, Effect of elastic distortions on solid-state amorphization at grain boundaries and dislocations, J. Phys. D Appl. Phys. 32 (1999) 2833.
[108] D. Clarke, G. Thomas, Grain boundary phases in a hot-pressed MgO fluxed silicon nitride, J. Am. Ceram. Soc. 60 (1977) 491–495.
[109] H. Wang, Y.M. Chiang, Thermodynamic stability of intergranular amorphous films in Bismuth-doped zinc oxide, J. Am. Ceram. Soc. 81 (1998) 89–96.
[110] J. Nie, J.M. Chan, M. Qin, N. Zhou, J. Luo, Liquid-like grain boundary complexion and sub-eutectic activated sintering in CuO-doped TiO2, Acta Mater. 130 (2017) 329–338.
[111] S.J. Dillon, M.P. Harmer, Relating grain-boundary complexion to grain-boundary kinetics I: calcia-doped alumina, J. Am. Ceram. Soc. 91 (2008) 2304–2313.
[112] V.K. Gupta, D.-H. Yoon, H.M. Meyer III, J. Luo, Thin intergranular films and solid-state activated sintering in nickel-doped tungsten, Acta Mater. 55 (2007) 3131–3142.
[113] X. Shi, J. Luo, Developing grain boundary diagrams as a materials science tool: a case study of nickel-doped molybdenum, Phys. Rev. B 84 (2011), 014105.
[114] J. Luo, V.K. Gupta, D.H. Yoon, H.M. Meyer, Segregation-induced grain boundary premelting in nickel-doped tungsten, Appl. Phys. Lett. 87 (2005) 231902.
[115] J. Luo, Grain boundary complexions: the interplay of premelting, prewetting, and multilayer adsorption, Appl. Phys. Lett. 95 (2009), 071911.
[116] S.J. Dillon, M. Tang, W.C. Carter, M.P. Harmer, Complexion: a new concept for kinetic engineering in materials science, Acta Mater. 55 (2007) 6208–6218.
[117] M. Tang, W.C. Carter, R.M. Cannon, Grain boundary transitions in binary alloys, Phys. Rev. Lett. 97 (2006), 075502.
[118] X. Shi, J. Luo, Grain boundary wetting and prewetting in Ni-doped Mo, Appl. Phys. Lett. 94 (2009) 251908.
[119] Z. Yu, Q. Wu, J.M. Rickman, H.M. Chan, M.P. Harmer, Atomic-resolution observation of Hf-doped alumina grain boundaries, Scr. Mater. 68 (2013) 703–706.
[120] S. Ma, K.M. Asl, C. Tansarawiput, P.R. Cantwell, M. Qi, M.P. Harmer, J. Luo, A grain boundary phase transition in Si–Au, Scr. Mater. 66 (2012) 203–206.
[121] A. Kundu, K.M. Asl, J. Luo, M.P. Harmer, Identification of a bilayer grain boundary complexion in Bi-doped Cu, Scr. Mater. 68 (2013) 146–149.
[122] J.D. Schuler, O.K. Donaldson, T.J. Rupert, Amorphous complexions enable a new region of high temperature stability in nanocrystalline Ni-W, Scr. Mater. 154 (2018) 49–53.
[123] C.M. Grigorian, T.J. Rupert, Thick Amorphous Complexion Formation and Extreme Thermal Stability in Ternary Nanocrystalline Cu-Zr-Hf Alloys, 2018 arXiv preprint arXiv:1808.00507.
[124] N. Zhou, T. Hu, J. Huang, J. Luo, Stabilization of nanocrystalline alloys at high temperatures via utilizing high-entropy grain boundary complexions, Scr. Mater. 124 (2016) 160–163.
[125] J. Weissmüller, Alloy effects in nanostructures, Nanostructured Mater. 3 (1993) 261–272.
[126] F. Abdeljawad, S.M. Foiles, Stabilization of nanocrystalline alloys via grain boundary segregation: a diffuse interface model, Acta Mater. 101 (2015) 159–171.
[127] S.G. Kim, Y.B. Park, Grain boundary segregation, solute drag and abnormal grain growth, Acta Mater. 56 (2008) 3739–3753.
[128] Z. Pan, T.J. Rupert, Effect of grain boundary character on segregation-induced structural transitions, Phys. Rev. B 93 (2016) 134113.
[129] J.D. Schuler, T.J. Rupert, Materials selection rules for amorphous complexion formation in binary metallic alloys, Acta Mater. 140 (2017) 196–205.
[130] D. Sundararaman, Nanocrystalline state and solid state amorphization, Mater. Sci. Eng., B 32 (1995) 307–313.
[131] I.A. Ovid'ko, A.G. Sheinerman, Irradiation-induced amorphization processes in nanocrystalline solids, Appl. Phys. A 81 (2005) 1083–1088.
[132] H. Jenniches, M. Klaua, H. Höche, J. Kirschner, Comparison of pulsed laser deposition and thermal deposition: improved layer-by-layer growth of Fe/Cu (111), Appl. Phys. Lett. 69 (1996) 3339–3341.
[133] T. Mukai, S. Suresh, K. Kita, H. Sasaki, N. Kobayashi, K. Higashi, A. Inoue, Nanostructured Al–Fe alloys produced by e-beam deposition: static and dynamic tensile properties, Acta Mater. 51 (2003) 4197–4208.
[134] K. Wasa, I. Kanno, H. Kotera, Handbook of Sputter Deposition Technology: Fundamentals and Applications for Functional Thin Films, Nano-Materials and MEMS, William Andrew, 2012.
[135] C. Cao, K. Huang, N. Zhao, Y. Sun, H. Bai, L. Gu, D. Zheng, W. Wang, Ultrahigh stability of atomically thin metallic glasses, Appl. Phys. Lett. 105 (2014), 011909.
[136] K. Huang, C. Cao, Y. Sun, J. Li, H. Bai, L. Gu, D. Zheng, W. Wang, Direct observation of atomic-level nucleation and growth processes from an ultrathin metallic glass films, J. Appl. Phys. 119 (2016), 014305.

[137] X. Huang, J. Guan, Z. Lin, B. Liu, S. Xing, W. Wang, J. Guo, Epitaxial growth and band structure of Te film on graphene, Nano Lett. 17 (2017) 4619–4623.
[138] J.-H. Chu, H.-W. Chen, Y.-C. Chan, J.-G. Duh, J.-W. Lee, J.S.-C. Jang, Modification of structure and property in Zr-based thin film metallic glass via processing temperature control, Thin Solid Films 561 (2014) 38–42.
[139] Z. Lee, C. Ophus, L. Fischer, N. Nelson-Fitzpatrick, K. Westra, S. Evoy, V. Radmilovic, U. Dahmen, D. Mitlin, Metallic NEMS components fabricated from nanocomposite Al–Mo films, Nanotechnology 17 (2006) 3063.
[140] C. Chen, J. Huang, H. Chou, Y. Lai, L. Chang, X. Du, J. Chu, T. Nieh, On the amorphous and nanocrystalline Zr–Cu and Zr–Ti co-sputtered thin films, J. Alloy. Comp. 483 (2009) 337–340.
[141] B. Braeckman, D. Depla, Structure formation and properties of sputter deposited Nbx-CoCrCuFeNi high entropy alloy thin films, J. Alloy. Comp. 646 (2015) 810–815.
[142] B. Braeckman, F. Misják, G. Radnóczi, D. Depla, The influence of Ge and in addition on the phase formation of CoCrCuFeNi high-entropy alloy thin films, Thin Solid Films 616 (2016) 703–710.
[143] Z.-C. Chang, S.-C. Liang, S. Han, Y.-K. Chen, F.-S. Shieu, Characteristics of TiVCrAlZr multi-element nitride films prepared by reactive sputtering, Nucl. Instrum. Methods Phys. Res. Sect. B Beam Interact. Mater. Atoms 268 (2010) 2504–2509.
[144] T. Chen, T. Shun, J. Yeh, M. Wong, Nanostructured nitride films of multi-element high-entropy alloys by reactive DC sputtering, Surf. Coat. Technol. 188 (2004) 193–200.
[145] C.-Y. Chuang, J.-W. Lee, C.-L. Li, J.P. Chu, Mechanical properties study of a magnetron-sputtered Zr-based thin film metallic glass, Surf. Coat. Technol. 215 (2013) 312–321.
[146] M. Apreutesei, P. Steyer, A. Billard, L. Joly-Pottuz, C. Esnouf, Zr–Cu thin film metallic glasses: an assessment of the thermal stability and phases' transformation mechanisms, J. Alloy. Comp. 619 (2015) 284–292.
[147] S. Kuan, H. Chou, J. Huang, Mechanical characteristics of Mg–Cu–Zr thin film metallic glasses, Surf. Coat. Technol. 231 (2013) 58–61.
[148] H. Gleiter, Nanocrystalline solids, J. Appl. Crystallogr. 24 (1991) 79–90.
[149] M. Mohri, D. Wang, J. Ivanisenko, H. Gleiter, H. Hahn, Investigation of the deposition conditions on the microstructure of TiZrCuPd nano-glass thin films, Mater. Char. 131 (2017) 140–147.
[150] P. Denis, S. Liu, H.-J. Fecht, Growth mode transition in Au-based thin film metallic glasses, Thin Solid Films 665 (2018) 29–35.
[151] N. Chen, D. Louzguine-Luzgin, G. Xie, P. Sharma, J. Perepezko, M. Esashi, A. Yavari, A. Inoue, Structural investigation and mechanical properties of a representative of a new class of materials: nanograined metallic glasses, Nanotechnology 24 (2013), 045610.
[152] N. Chen, R. Frank, N. Asao, D. Louzguine-Luzgin, P. Sharma, J. Wang, G. Xie, Y. Ishikawa, N. Hatakeyama, Y. Lin, Formation and properties of Au-based nanograined metallic glasses, Acta Mater. 59 (2011) 6433–6440.
[153] Z. Śniadecki, D. Wang, Y. Ivanisenko, V. Chakravadhanula, C. Kübel, H. Hahn, H. Gleiter, Nanoscale morphology of Ni50Ti45Cu5 nanoglass, Mater. Char. 113 (2016) 26–33.
[154] H. Gleiter, Our thoughts are ours, their ends none of our own: are there ways to synthesize materials beyond the limitations of today? Acta Mater. 56 (2008) 5875–5893.
[155] A. Inoue, H. Tomioka, T. Masumoto, Mechanical properties of ductile Fe-Ni-Zr and Fe-Ni-Zr (Nb or Ta) amorphous alloys containing fine crystalline particles, J. Mater. Sci. 18 (1983) 153–160.
[156] K. YH, K. Hiraga, A. Inoue, T. Masumoto, Crystallization and high mechanical strength of Al-based amorphous alloys, Mater. Trans., JIM 35 (1994) 293–302.
[157] G. Choi, Y. Kim, H. Cho, A. Inoue, T. Masumoto, Ultrahigh tensile strength of amorphous Al-Ni-(Nd, Gd)-Fe alloys containing nanocrystalline Al particles, Scr. Metall. Mater. 33 (1995) 1301–1306.
[158] Y.-H. Kim, A. Inoue, T. Masumoto, Increase in mechanical strength of Al–Y–Ni amorphous alloys by dispersion of nanoscale fcc-Al particles, Mater. Trans., JIM 32 (1991) 331–338.
[159] Y.-H. Kim, A. Inoue, T. Masumoto, Ultrahigh mechanical strengths of Al88Y2Ni10− xMx (M= Mn, Fe or Co) amorphous alloys containing nanoscale fcc-Al particles, Mater. Trans., JIM 32 (1991) 599–608.
[160] A. Inoue, Amorphous, nanoquasicrystalline and nanocrystalline alloys in Al-based systems, Prog. Mater. Sci. 43 (1998) 365–520.
[161] C. Fan, A. Inoue, Improvement of mechanical properties by precipitation of nanoscale compound particles in Zr–Cu–Pd–Al amorphous alloys, Mater. Trans., JIM 38 (1997) 1040–1046.
[162] C. Fan, A. Takeuchi, A. Inoue, Preparation and mechanical properties of Zr-based bulk nanocrystalline alloys containing compound and amorphous phases, Mater. Trans., JIM 40 (1999) 42–51.
[163] J. Eckert, J. Das, S. Pauly, C. Duhamel, Mechanical properties of bulk metallic glasses and composites, J. Mater. Res. 22 (2007) 285–301.
[164] L. Xing, J. Eckert, W. Löser, L. Schultz, High-strength materials produced by precipitation of icosahedral quasicrystals in bulk Zr–Ti–Cu–Ni–Al amorphous alloys, Appl. Phys. Lett. 74 (1999) 664–666.
[165] Y.C. Kim, J.H. Na, J.M. Park, D.H. Kim, J.K. Lee, W.T. Kim, Role of nanometer-scale quasicrystals in improving the mechanical behavior of Ti-based bulk metallic glasses, Appl. Phys. Lett. 83 (2003) 3093–3095.
[166] Q. Zhang, W. Zhang, G. Xie, D. Louzguine-Luzgin, A. Inoue, Stable flowing of localized shear bands in soft bulk metallic glasses, Acta Mater. 58 (2010) 904–909.
[167] H.W. Bi, A. Inoue, F.F. Han, Y. Han, F.L. Kong, S.L. Zhu, E. Shalaan, F. Al-Marzouki, A.L. Greer, Novel deformation-induced polymorphic crystallization and softening of Al-based amorphous alloys, Acta Mater. 147 (2018) 90–99.
[168] Z.C. Cordero, B.E. Knight, C.A. Schuh, Six decades of the Hall–Petch effect – a survey of grain-size strengthening studies on pure metals, Int. Mater. Rev. 61 (2016) 495–512.
[169] C.S. Pande, K.P. Cooper, Nanomechanics of Hall–Petch relationship in nanocrystalline materials, Prog. Mater. Sci. 54 (2009) 689–706.
[170] J. Schiøtz, F.D. Di Tolla, K.W. Jacobsen, Softening of nanocrystalline metals at very small grain sizes, Nature 391 (1998) 561–563.
[171] R. Bohn, T. Klassen, R. Bormann, Room temperature mechanical behavior of silicon-doped TiAl alloys with grain sizes in the nano- and submicron-range, Acta Mater. 49 (2001) 299–311.
[172] S. Özerinç, K. Tai, N.Q. Vo, P. Bellon, R.S. Averback, W.P. King, Grain boundary doping strengthens nanocrystalline copper alloys, Scr. Mater. 67 (2012) 720–723.
[173] F. Tang, D.S. Gianola, M.P. Moody, K.J. Hemker, J.M. Cairney, Observations of grain boundary impurities in nanocrystalline Al and their influence on microstructural stability and mechanical behaviour, Acta Mater. 60 (2012) 1038–1047.
[174] N.Q. Vo, J. Schäfer, R.S. Averback, K. Albe, Y. Ashkenazy, P. Bellon, Reaching theoretical strengths in nanocrystalline Cu by grain boundary doping, Scr. Mater. 65 (2011) 660–663.
[175] C. Xiao, R.A. Mirshams, S.H. Whang, W.M. Yin, Tensile behavior and fracture in nickel and carbon doped nanocrystalline nickel, Mater. Sci. Eng.: A 301 (2001) 35–43.
[176] A. Khalajhedayati, Z. Pan, T.J. Rupert, Manipulating the interfacial structure of nanomaterials to achieve a unique combination of strength and ductility, Nat. Commun. 7 (2016) 10802.
[177] D.S. Gianola, Z. Lee, C. Ophus, E.J. Luber, D. Mitlin, U. Dahmen, K.J. Hemker, V.R. Radmilović, Tensile behavior of Al1−xMox crystalline and amorphous thin films, Acta Mater. 61 (2013) 1432–1443.
[178] C. Fan, A. Inoue, Ductility of bulk nanocrystalline composites and metallic glasses at room temperature, Appl. Phys. Lett. 77 (2000) 46–48.
[179] C.-M. Lee, S.-W. Chae, H.-J. Kim, J.-C. Lee, Role of nanocrystals on the plasticity of amorphous alloy, Met. Mater. Int. 13 (2007) 191–196.
[180] H.S. Kim, S.I. Hong, A model of the ductile–brittle transition of partially crystallized amorphous Al–Ni–Y alloys, Acta Mater. 47 (1999) 2059–2066.
[181] F. Li, T. Liu, T. Wang, A. Wang, J. Wang, Y. Yang, Understanding yielding and the unusual ductile-brittle-ductile transition in Fe-based amorphous nanocrystalline alloy: a combined micromechanical and thermodynamic study, J. Mech. Phys. Solids 132 (2019) 103681.
[182] J.E. Ludy, T.J. Rupert, Amorphous intergranular films act as ultra-efficient point defect sinks during collision cascades, Scr. Mater. 110 (2016) 37–40.
[183] C.J. Gilbert, R.O. Ritchie, W.L. Johnson, Fracture toughness and fatigue-crack propagation in a Zr–Ti–Ni–Cu–Be bulk metallic glass, Appl. Phys. Lett. 71 (1997) 476–478.
[184] J. Schroers, W.L. Johnson, Ductile bulk metallic glass, Phys. Rev. Lett. 93 (2004) 255506.
[185] N. Nagendra, U. Ramamurty, T.T. Goh, Y. Li, Effect of crystallinity on the impact toughness of a La-based bulk metallic glass, Acta Mater. 48 (2000) 2603–2615.
[186] J. Ketkaew, Z. Liu, W. Chen, J. Schroers, Critical crystallization for embrittlement in metallic glasses, Phys. Rev. Lett. 115 (2015) 265502.
[187] Y. Yang, B. Imasogie, G.J. Fan, P.K. Liaw, W.O. Soboyejo, Fatigue and fracture of a bulk nanocrystalline NiFe alloy, Metall. Mater. Trans. A 39 (2008) 1145–1156.
[188] R.A. Mirshams, C.H. Xiao, S.H. Whang, W.M. Yin, R-Curve characterization of the fracture toughness of nanocrystalline nickel thin sheets, Mater. Sci. Eng.: A 315 (2001) 21–27.
[189] A. Wang, C. Zhao, A. He, H. Men, C. Chang, X. Wang, Composition design of high Bs Fe-based amorphous alloys with good amorphous-forming ability, J. Alloy. Comp. 656 (2016) 729–734.
[190] R. Schäfer, The Magnetic Microstructure of Nanostructured Materials. Nanoscale Magnetic Materials and Applications, Springer, 2009, pp. 275–307.
[191] G. Herzer, Nanocrystalline soft magnetic alloys, Handb. Magn. Mater. 10 (1997) 415–462.
[192] G. Herzer, Modern soft magnets: amorphous and nanocrystalline materials, Acta Mater. 61 (2013) 718–734.
[193] M. Ohta, Y. Yoshizawa, Cu addition effect on soft magnetic properties in Fe–Si–B alloy system, J. Appl. Phys. 103 (2008), 07E722.
[194] A. Makino, T. Kubota, K. Yubuta, A. Inoue, A. Urata, H. Matsumoto, S. Yoshida, Low core losses and magnetic properties of Fe85-86Si1-2B8P4Cu1 nanocrystalline alloys with high B for power applications, J. Appl. Phys. 109 (2011), 07A302.
[195] A. Makino, Nanocrystalline soft magnetic Fe-Si-B-P-Cu alloys with high B of 1.8-1.9T contributable to energy saving, IEEE Trans. Magn. 48 (2012) 1331–1335.
[196] R. Hasegawa, Applications of Amorphous Magnetic Alloys. Properties and Applications of Nanocrystalline Alloys from Amorphous Precursors, Springer, 2005, pp. 189–198.
[197] M. Kuhnt, M. Marsilius, T. Strache, C. Polak, G. Herzer, Magnetostriction of nanocrystalline (Fe,Co)-Si-B-P-Cu alloys, Scr. Mater. 130 (2017) 46–48.

[198] O. Gutfleisch, M.A. Willard, E. Brück, C.H. Chen, S.G. Sankar, J.P. Liu, Magnetic materials and devices for the 21st century: stronger, lighter, and more energy efficient, Adv. Mater. 23 (2011) 821–842.
[199] I. Jain, C. Lal, A. Jain, Hydrogen storage in Mg: a most promising material, Int. J. Hydrogen Energy 35 (2010) 5133–5144.
[200] J.-C. Crivello, B. Dam, R. Denys, M. Dornheim, D. Grant, J. Huot, T.R. Jensen, P. De Jongh, M. Latroche, C. Milanese, Review of magnesium hydride-based materials: development and optimisation, Appl. Phys. A 122 (2016) 97.
[201] S. Orimo, H. Fujii, K. Ikeda, Notable hydriding properties of a nanostructured composite material of the Mg2Ni-H system synthesized by reactive mechanical grinding, Acta Mater. 45 (1997) 331–341.
[202] M. Au, Hydrogen storage properties of magnesium based nanostructured composite materials, Mater. Sci. Eng., B 117 (2005) 37–44.
[203] Y.-h. Zhang, B.-w. Li, Z.-h. Ma, S.-h. Guo, Y. Qi, X.-l. Wang, Improved hydrogen storage behaviours of nanocrystalline and amorphous Mg2Ni-type alloy by Mn substitution for Ni, Int. J. Hydrogen Energy 35 (2010) 11966–11974.
[204] S. Kalinichenka, L. Röntzsch, B. Kieback, Structural and hydrogen storage properties of melt-spun Mg–Ni–Y alloys, Int. J. Hydrogen Energy 34 (2009) 7749–7755.
[205] H. Lin, L. Ouyang, H. Wang, D. Zhao, W. Wang, D. Sun, M. Zhu, Hydrogen storage properties of Mg–Ce–Ni nanocomposite induced from amorphous precursor with the highest Mg content, Int. J. Hydrogen Energy 37 (2012) 14329–14335.
[206] L. Song, W. Li, G. Wang, M. Zhang, K. Tao, A new route to prepare supported nickel phosphide/silica–alumina hydrotreating catalysts from amorphous alloys, Catal. Today 125 (2007) 137–142.
[207] Y. Deng, Y. Yang, L. Ge, W. Yang, K. Xie, Preparation of magnetic Ni-P amorphous alloy microspheres and their catalytic performance towards thermal decomposition of ammonium perchlorate, Appl. Surf. Sci. 425 (2017) 261–271.
[208] H. Hu, M. Qiao, S. Wang, K. Fan, H. Li, B. Zong, X. Zhang, Structural and catalytic properties of skeletal Ni catalyst prepared from the rapidly quenched Ni50Al50 alloy, J. Catal. 221 (2004) 612–618.
[209] L. Mihailov, M. Redzheb, T. Spassov, Selective dissolution of amorphous and nanocrystalline Zr2Ni, Corros. Sci. 74 (2013) 308–313.
[210] T. Burchardt, V. Hansen, T. Våland, Microstructure and catalytic activity towards the hydrogen evolution reaction of electrodeposited NiPx alloys, Electrochim. Acta 46 (2001) 2761–2766.
[211] J. Jiang, R. Zhai, X. Bao, Electrocatalytic properties of Cu–Zr amorphous alloy towards the electrochemical hydrogenation of nitrobenzene, J. Alloy. Comp. 354 (2003) 248–258.
[212] D. He, L. Zhang, D. He, G. Zhou, Y. Lin, Z. Deng, X. Hong, Y. Wu, C. Chen, Y. Li, Amorphous nickel boride membrane on a platinum–nickel alloy surface for enhanced oxygen reduction reaction, Nat. Commun. 7 (2016) 12362.
[213] Z. Dan, F. Qin, T. Wada, S.-i. Yamaura, G. Xie, Y. Sugawara, I. Muto, A. Makino, N. Hara, Nanoporous palladium fabricated from an amorphous Pd42. 5Cu30Ni7. 5P20 precursor and its ethanol electro-oxidation performance, Electrochim. Acta 108 (2013) 512–519.
[214] Z. Qi, H. Geng, X. Wang, C. Zhao, H. Ji, C. Zhang, J. Xu, Z. Zhang, Novel nanocrystalline PdNi alloy catalyst for methanol and ethanol electrooxidation in alkaline media, J. Power Sources 196 (2011) 5823–5828.
[215] M. Pisarek, M. Łukaszewski, P. Winiarek, P. Kędzierzawski, M. Janik-Czachor, Catalytic activity of Cr-or Co-modified Ni-based rapidly quenched alloys in the hydrogenation of isophorone, Appl. Catal. Gen. 358 (2009) 240–248.
[216] L. Mihailov, T. Spassov, M. Bojinov, Effect of microstructure on the electrocatalytic activity for hydrogen evolution of amorphous and nanocrystalline Zr–Ni alloys, Int. J. Hydrogen Energy 37 (2012) 10499–10506.
[217] R. Hauert, J. Patscheider, From alloying to nanocomposites—improved performance of hard coatings, Adv. Eng. Mater. 2 (2000) 247–259.
[218] T. Gloriant, Microhardness and abrasive wear resistance of metallic glasses and nanostructured composite materials, J. Non-Cryst. Solids 316 (2003) 96–103.
[219] J. Wang, B. Choi, T. Nieh, C. Liu, Nano-scratch behavior of a bulk Zr–10Al–5Ti–17.9 Cu–14.6 Ni amorphous alloy, J. Mater. Res. 15 (2000) 913–922.
[220] J.-b. Cheng, X.-b. Liang, B.-s. Xu, Y.-x. Wu, Formation and properties of Fe-based amorphous/nanocrystalline alloy coating prepared by wire arc spraying process, J. Non-Cryst. Solids 355 (2009) 1673–1678.
[221] B. Movahedi, M. Enayati, C. Wong, Structural and thermal behavior of Fe-Cr-Mo-PBC-Si amorphous and nanocrystalline HVOF coatings, J. Therm. Spray Technol. 19 (2010) 1093–1099.
[222] Z.-y. Piao, B.-s. Xu, H.-d. Wang, D.-h. Wen, Characterization of Fe-based alloy coating deposited by supersonic plasma spraying, Fusion Eng. Des. 88 (2013) 2933–2938.
[223] Q. Zhu, X. Wang, S. Qu, Z. Zou, Microstructure and wear properties of laser clad Fe based amorphous composite coatings, Surf. Eng. 25 (2009) 201–205.
[224] X. Hong, Y. Tan, C. Zhou, T. Xu, Z. Zhang, Microstructure and tribological properties of Zr-based amorphous-nanocrystalline coatings deposited on the surface of titanium alloys by Electrospark Deposition, Appl. Surf. Sci. 356 (2015) 1244–1251.
[225] J.M. Silveyra, E. Ferrara, D.L. Huber, T.C. Monson, Soft magnetic materials for a sustainable and electrified world, Science 362 (2018) eaao0195.
[226] A. Krings, A. Boglietti, A. Cavagnino, S. Sprague, Soft magnetic material status and trends in electric machines, IEEE Trans. Ind. Electron. 64 (2016) 2405–2414.
[227] T. Kauder, K. Hameyer, Performance factor comparison of nanocrystalline, amorphous, and crystalline soft magnetic materials for medium-frequency applications, IEEE Trans. Magn. 53 (2017) 1–4.
[228] http://www.atmcn.com/cpyfw/cpdh/fjnmjdc/fjnmjdc/namijdc/2015/1222/3060.html.
[229] W. Shen, F. Wang, D. Boroyevich, C.W. Tipton, Loss characterization and calculation of nanocrystalline cores for high-frequency magnetics applications, in: APEC 07-Twenty-Second Annual IEEE Applied Power Electronics Conference and Exposition, IEEE, 2007, pp. 90–96.
[230] A.M. Leary, P.R. Ohodnicki, M.E. McHenry, Soft magnetic materials in high-frequency, high-power conversion applications, JOM 64 (2012) 772–781.
[231] R. Hasegawa, Present status of amorphous soft magnetic alloys, J. Magn. Magn. Mater. 215–216 (2000) 240–245.
[232] Y. Naitoh, T. Bitoh, T. Hatanai, A. Makino, A. Inoue, T. Masumoto, Development of common mode choke coil made of new nanocrystalline soft magnetic alloy“ NANOPERM˙[○! R]”, Sci. Rep. Res. Inst. Tohoku Univ. Ser. A Phys. Chem. Metall. 43 (1997) 161–165.
[233] B.T. Naitoh Y, T. Hatanai, Applications of nanocrystalline soft magnetic Fe-MB (M= Zr, Nb) alloys, Nanostructured Mater. 8 (8) (1997) 987–995.
[234] http://www.atmcn.com/cpyfw/cpdh/fjnmjdc/fjnmjqj/.
[235] R.M. Del Vecchio, R. Del Vecchio, B. Poulin, P.T. Feghali, D.M. Shah, R. Ahuja, Transformer Design Principles With Applications 3e, CRC press, 2017.
[236] A. De Almeida, B. Santos, F. Martins, Energy-efficient distribution transformers in Europe: impact of Ecodesign regulation, Energy Eff. 9 (2016) 401–424.
[237] G.Y. Rabiul Islam M, Z. Wei Lin, An amorphous alloy core medium frequency magnetic-link for medium voltage photovoltaic inverters, J. Appl. Phys. 115 (17) (2014) 17E710.
[238] M. Ferch, Application overview of nanocrystalline inductive components in today's power electronic systems, Proc. Soft Magn. Mater. Conf. (A1–01) (2013).
[239] A. Inoue, A. Takeuchi, A. Makino, T. Masumoto, Hard magnetic properties of Fe-Nd-B alloys containing intergranular amorphous phase, IEEE Trans. Magn. 31 (1995) 3626–3628.
[240] A. Inoue, A. Takeuchi, A. Makino, T. Masumoto, Soft and hard magnetic properties of nanocrystalline Fe-MB (M= Zr, Nd) base alloys containing intergranular amorphous phase, Sci. Rep. Res. Inst. Tohoku Univ. Ser. A Phys. Chem. Metall. 42 (1996) 143–156.
[241] W. Zhang, M. Matsushita, A. Inoue, Hard magnetic properties of Fe–Co–Nd–Dy–B nanocrystalline alloys containing residual amorphous phase, J. Appl. Phys. 89 (2001) 492–495.
[242] Y. Jin, R. Li, H. Xu, X.-B. Chen, T. Zhang, A new strategy to fabricate nanoporous iron-based metallic glasses: selective phase tailoring of amorphous-nanocrystalline composite alloys through electrochemical dissolution, Scr. Mater. 133 (2017) 14–18.
[243] C. Fu, L. Xu, Z. Dan, A. Makino, N. Hara, F. Qin, H. Chang, Structural inheritance and redox performance of nanoporous electrodes from nanocrystalline Fe85. 2B10-14P0-4Cu0. 8 alloys, Nanomaterials 7 (2017) 141.
[244] C. Fu, L. Xu, Z. Dan, F. Qin, A. Makino, H. Chang, N. Hara, Annealing effect of amorphous Fe-Si-BP-Cu precursors on microstructural evolution and redox behavior of nanoporous counterparts, J. Alloy. Comp. 726 (2017) 810–819.
[245] H. Zhang, J. Fornell, Y. Feng, I. Golvano, M.D. Baró, E. Pellicer, J. Sort, Inducing surface nanoporosity on Fe-based metallic glass matrix composites by selective dealloying, Mater. Char. 153 (2019) 46–51.
[246] Y. Ye, Z. Liu, W. Liu, D. Zhang, Y. Wang, H. Zhao, L. Wang, X. Li, Bias design of amorphous/nanocrystalline CrAlSiN films for remarkable anti-corrosion and anti-wear performances in seawater, Tribol. Int. 121 (2018) 410–419.
[247] J. Xu, Z. Chen, J. Tao, S. Jiang, Z. Liu, Z. Xu, Corrosion behavior of amorphous/nanocrystalline Al-Cr-Fe film deposited by double glow plasmas technique, Sci. China Ser. E Technol. Sci. 52 (2009) 1225.
[248] C. Tan, H. Zhu, T. Kuang, J. Shi, H. Liu, Z. Liu, Laser cladding Al-based amorphous-nanocrystalline composite coatings on AZ80 magnesium alloy under water cooling condition, J. Alloy. Comp. 690 (2017) 108–115.
[249] J. Sweitzer, G. Shiflet, J.R. Scully, Localized corrosion of Al90Fe5Gd5 and Al87Ni8. 7Y4. 3 alloys in the amorphous, nanocrystalline and crystalline states: resistance to micrometer-scale pit formation, Electrochim. Acta 48 (2003) 1223–1234.
[250] E. Sikora, X. Wei, B. Shaw, Corrosion behavior of nanocrystalline bulk Al-Mg-based alloys, Corrosion 60 (2004) 387–398.
[251] A.M. Lucente, J.R. Scully, Localized corrosion of Al-based amorphous-nanocrystalline alloys with solute-lean nanocrystals: pit stabilization, J. Electrochem. Soc. 155 (2008) C234–C243.
[252] S. Wang, Z. Zhang, Y. Gong, G. Nie, Microstructures and corrosion resistance of Fe-based amorphous/nanocrystalline coating fabricated by laser cladding, J. Alloy. Comp. 728 (2017) 1116–1123.
[253] C. Souza, D. Ribeiro, C. Kiminami, Corrosion resistance of Fe-Cr-based amorphous alloys: an overview, J. Non-Cryst. Solids 442 (2016) 56–66.
[254] Y.-j. Qin, Y.-p. Wu, J.-f. Zhang, W.-m. Guo, H. Sheng, L.-y. Chen, Long-term corrosion behavior of HVOF sprayed FeCrSiBMn amorphous/nanocrystalline coating, Trans. Nonferrous Metals Soc. China 25 (2015) 1144–1150.
[255] W. Guo, Y. Wu, J. Zhang, S. Hong, G. Li, G. Ying, J. Guo, Y. Qin, Fabrication and characterization of thermal-sprayed Fe-based amorphous/nanocrystalline

composite coatings: an overview, J. Therm. Spray Technol. 23 (2014) 1157–1180.
[256] J. Cheng, Z. Wang, B. Xu, Wear and corrosion behaviors of FeCrBSiNbW amorphous/nanocrystalline coating prepared by arc spraying process, J. Therm. Spray Technol. 21 (2012) 1025–1031.
[257] A. Baron, D. Szewieczek, G. Nawrat, Corrosion of amorphous and nanocrystalline Fe-based alloys and its influence on their magnetic behavior, Electrochim. Acta 52 (2007) 5690–5695.
[258] Y.N. Bekish, S. Poznyak, L. Tsybulskaya, T. Gaevskaya, Electrodeposited Ni–B alloy coatings: structure, corrosion resistance and mechanical properties, Electrochim. Acta 55 (2010) 2223–2231.
[259] A. Dent, A. Horlock, D. McCartney, S. Harris, The corrosion behavior and microstructure of high-velocity oxy-fuel sprayed nickel-base amorphous/nanocrystalline coatings, J. Therm. Spray Technol. 8 (1999) 399–404.
[260] Y.-Y. Li, F.-B. Wu, Microstructure and corrosion characteristics of CrN/NiP sputtering thin films, Thin Solid Films 518 (2010) 7527–7531.
[261] J. Farmer, J.-S. Choi, C. Saw, J. Haslam, D. Day, P. Hailey, T. Lian, R. Rebak, J. Perepezko, J. Payer, Iron-based amorphous metals: high-performance corrosion-resistant material development, Metall. Mater. Trans. A 40 (2009) 1289–1305.
[262] J.R. Scully, A. Gebert, J.H. Payer, Corrosion and related mechanical properties of bulk metallic glasses, J. Mater. Res. 22 (2007) 302–313.
[263] D. Wang, S. Wang, J. Wang, Relationship between amorphous structure and corrosion behaviour in a Zr–Ni metallic glass, Corros. Sci. 59 (2012) 88–95.
[264] P. Gostin, A. Gebert, L. Schultz, Comparison of the corrosion of bulk amorphous steel with conventional steel, Corros. Sci. 52 (2010) 273–281.
[265] A.M. Lucente, J.R. Scully, Pitting and alkaline dissolution of an amorphous–nanocrystalline alloy with solute-lean nanocrystals, Corros. Sci. 49 (2007) 2351–2361.
[266] W.C. Johnson, P. Zhou, A. Lucente, J. Scully, Composition profiles around solute-lean, spherical nanocrystalline precipitates in an amorphous matrix: implications for corrosion resistance, Metall. Mater. Trans. A 40 (2009) 757–767.